RSC Sustainability

ROYAL SOCIETY OF CHEMISTRY

PAPER

View Article Online
View Journal | View Issue

Cite this: *RSC Sustainability*, 2026, **4**, 381

Kinetic analysis and optimization of sonoreactor process for production of humic and fulvic acids from various coal feedstocks

Redhwan Al-Akbari, [a] Abdallah D. Manasrah [b] and Nashaat N. Nassar *[a]

Developing high-yield, non-combustion applications for low-rank coals is critical for their sustainable utilization. This study demonstrates a rapid ultrasonic process, using H_2O_2 in an alkaline medium, to efficiently convert four distinct low-rank coals (humalite, leonardite, peat, and subbituminous) into valuable humic and fulvic acids. The process achieved high conversions for all feedstocks, with the more oxidized coals, leonardite and humalite, showing the highest conversions (91% and 88%, respectively) and humic acid yields (81% for both). A double triangular lump kinetic model revealed that ultrasonication preferentially favors the reaction pathway toward humic acids over fulvic acids and CO_2, with lower apparent activation energies for humic acid formation across all feedstocks. This was most pronounced for humalite and leonardite (51 and 58 kJ mol^{-1}). Spectroscopic and titrimetric analyses confirmed the successful incorporation of oxygen-containing functional groups (COOH and OH) into the coal structure, driven by the attack of $^{\bullet}OH$ radicals generated during sonication. Overall, this work establishes an efficient and selective pathway for producing humic acids from low-rank coals, presenting a scalable technology for converting these resources into high-value soil amendments.

Received 17th September 2025
Accepted 16th November 2025

DOI: 10.1039/d5su00752f

rsc.li/rscsus

Sustainability spotlight

Low-rank coal is abundant but traditionally burnt for power, releasing large amounts of greenhouse gases and pollutants. We present an ultrasonic conversion process that transforms these coals into humic- and fulvic-acid analogues under mild conditions, cutting energy demand and CO_2 emissions compared with conventional extraction or combustion. The resulting bioactive products can serve as soil amendments, improving fertility and supporting circular nutrient management. This scalable approach turns a high-emission fossil resource into value-added materials, advancing resource efficiency and waste reduction. The work supports UN Sustainable Development Goals 12 (Responsible Consumption and Production), 13 (Climate Action), and 15 (Life on Land) by enabling lower-emission coal valorization, enhancing soil health, and promoting sustainable resource use.

1. Introduction

Governments and corporations are actively working to phase out coal, which is typically used in electricity generation, as part of the transition to low-carbon energy systems, to mitigate the impacts of climate change.[1] This transition requires significant investment in clean energy technologies. One area of focus is the utilization of coal for producing value-added products, which presents an opportunity to repurpose this abundant resource more sustainably. However, the complex and heterogeneous nature of coal can impose technical challenges for its direct conversion to valuable products. These challenges include low selectivity, limited yield, and challenging separation processes, all of which severely limit the efficiency and economic viability of coal utilization.[2] Addressing these gaps requires the development of technologies capable of achieving high yields while minimizing greenhouse gas (GHG) emissions.

Low-rank coals, such as subbituminous, leonardite, humalite, and peat (precursor of coal), are characterized by lower carbon content and higher moisture content compared to higher-rank coals like bituminous and anthracite.[3] These coals are typically used for power generation and serve as an important source of energy, particularly in developing countries with limited access to other sources of energy. However, the distinct physical and chemical characteristics of these coals, such as their lower heating value and higher emissions profile, pose challenges to their utilization.[4] Due to their lower heating value, larger amounts are needed to generate the same amount of energy compared to higher-rank coals. Additionally, their combustion releases higher levels of volatile organic compounds, contributing to air pollution and emissions of GHG.[5] The high ash content tends to deposit on furnace walls, leading to corrosion and a reduction in heat transfer efficiency.

[a]*Department of Chemical and Petroleum Engineering, University of Calgary, 2500 University Drive Northwest, Calgary, Alberta, T2N 1N4, Canada. E-mail: nassar@ucalgary.ca*

[b]*Carbon OxyTech Inc., Calgary, Alberta, Canada, T2L 1Y8. Tel: +1-403-641-0111. E-mail: manasrah@carbonoxytech.com*

In this study, we focused on four types of coals, namely: leonardite, humalite, peat, and subbituminous coals, to convert them into humic and fulvic acid analogs. Leonardite is a naturally oxidized variant of lignite coal,[6] while humalite is a weathered by-product of subbituminous coal and carbonaceous shales.[7] Peat, on the other hand, is a partially decomposed accumulation of plant material in wetland environments characterized by high water content and low carbonization, resulting in a fibrous and organic-rich substance.[8] While peat is not classified in some literature as a low rank coal, it is nevertheless a precursor to low rank coals and exhibit similar characteristics chemical and physical. Subbituminous coal has a dull black appearance, relatively high moisture content, lower carbon content compared to bituminous coal, and a slightly higher energy content than lignite.[9] The selection of these four feedstocks allows the evaluation of diverse physical and chemical attributes and enhances the robustness of the proposed process in addressing the variability inherent to these feedstocks. By focusing on these variations, this study aims to develop a reliable method for transforming the four feedstocks into humic and fulvic acid analogs, thereby providing a sustainable utilization pathway with a lower environmental impact.

Humic substances are complex organic molecules that play roles in soil chemistry and plant growth.[10] The naturally occurring humic substances are primarily derived from the decomposition of plants, animal residues, and coals and are composed of a variety of molecules, including humic acids, fulvic acids, and humin.[11] Extraction of humic substances from soil or coals involves several sequential steps, which can include chemical, physical, and biological processes.[12] A variety of methods have been established for extracting humic substances from sources like coal and soil, including hydrothermal extraction, solid-phase activation process, bioconversion, non-catalytic oxidation with oxygen, oxidation with H_2O_2, alkaline extraction, water-oxygen system, and the International Humic Substance Society method.[13–17] While foundational to the field, a critical assessment of these processes reveals significant limitations that impede their efficiency and sustainability. A primary challenge is process inefficiency, often characterized by low yields and prohibitively long reaction times. Reported humic acid yields vary drastically depending on the feedstock, from as low as 5–15% for compost to a maximum of 80–90% for high-quality leonardite, with most sources falling somewhere in between.[18–20] Moreover, achieving these higher yields often requires extreme processing conditions or multi-day reaction times, as seen in thermophilic aerobic processes that can take up to two days.[21] For instance, even advanced KOH-hydrothermal extractions can require over seven hours of processing.[13] Compounding these issues is the reliance of many methods on harsh chemical reagents like HCl, HNO_3, and various organic solvents. This dependence not only introduces environmental risks associated with chemical waste disposal but also adds significant operational complexity and cost. Consequently, there remains a pressing need for an alternative production strategy that is simultaneously rapid, high-yield, and environmentally friendly.

Building upon these goals, the ultrasonication process has recently emerged as a promising technological approach for the transformation of coals into humic substances.[22,23] While our previous study established the proof-of-concept for this technique using a single lignite feedstock, the present study makes several significant new contributions.[23] First, we demonstrate the broad applicability and versatility of the process by extending it to four distinct low-rank coals: humalite, leonardite, subbituminous, and peat, each with unique physicochemical properties. Second, we develop a comprehensive lumped kinetic model for each feedstock to explain the reaction pathways and quantify the rates of formation for all major products. Finally, by correlating these kinetic parameters with the elemental composition of the feedstocks, we provide direct, quantitative evidence for the underlying reaction mechanism, advancing beyond the qualitative observations of prior work. This effort validates the versatility of ultrasonication in generating humic and fulvic acid analogs from various feedstocks. The employment of ultrasonic waves as an enhancement mechanism offers a reduction in reaction time and an increase in conversion efficiency relative to existing techniques. Ultrasonication facilitates the breakdown of LRC by cavitation, a process where rapid pressure changes create microbubbles that collapse, releasing intense energy.[24] The collapse of these cavitation bubbles generates extreme localized conditions, with temperatures reaching up to 5000 K and pressures exceeding 1000 atmospheres.[25] These conditions provide sufficient energy to break the molecular bonds of water (H_2O) and other dissolved gases such as O_2, which can disassociate into $^{\bullet}O$ radicals that react with H_2O, leading to the formation of highly reactive hydroxyl radicals. The generation of $^{\bullet}OH$ radicals in an ultrasonic horn reactor is a critical part in the mechanism of the formation of humic and fulvic acid analogs from LRC. Comprehensive characterization techniques, including FTIR, TGA, CHN, ^1H NMR and potentiometric titrations, confirmed the incorporation of oxygen into the LRC molecular structure through the formation of new carboxylic and phenolic functional groups. Reaction kinetics revealed that more oxidized types of LRC, such as humalite and leonardite, are easier to convert to humic and fulvic acid analogs, evident in lower activation energies. Moreover, reaction pathways to forming CO_2 were found to be the least favourable among the six reaction pathways in all four types of LRC investigated. Optimizing reaction and reactor parameters demonstrated the effectiveness of ultrasonication, achieving humic acid yields of 66–81%, depending on the maturity of the LRC. The process minimized CO_2 emissions and significantly reduced reaction time to 40 min. This study emphasizes the potential of ultrasonication as a scalable, efficient, and environmentally sustainable method for the conversion of LRCs into high-value humic substances. The research directly aligns with several United Nations Sustainable Development Goals (SDGs). Specifically, our approach contributes to SDG 13 (Climate Action) by creating a low-emission alternative to coal combustion, supports SDG 12 (Responsible Consumption and Production) by upcycling a fossil resource into high-value materials, and advances SDG

15 (Life on Land) by producing amendments that enhance soil health and agricultural sustainability.

2. Materials and methods

2.1. Chemicals and reagents

Four types of LRCs were used in this study, namely subbituminous coal, humalite, leonardite and peat. Subbituminous coal sample was obtained from Dodds Coal Mining Company Ltd (Alberta, Canada), and leonardite was obtained from Leonardite Products LLC (North Dakota, USA). Humalite was obtained from WestMET Group Canada Ltd (Alberta, Canada). Peat was sourced locally from a store in Calgary, Alberta. Humalite, leonardite, and peat were received in powdered form, whereas subbituminous coal sample was initially crushed with a hammer and subsequently processed in a mill grinder (2000*g* Electric Grain Grinder Mill, Marada) to produce fine powder with particle sizes ranging between 75 and 590 μm. Hydrogen peroxide (30 wt% H_2O_2), procured from VWR (Ontario, Canada), used as an oxidizing agent. In accordance with the principles of green chemistry, hydrogen peroxide was selected as the oxidant due to its high atom economy and the generation of water as its sole byproduct. The use of a dilute (3 wt%) solution ensures that the process is safe and poses a negligible environmental burden at the laboratory scale, as any residual oxidant readily decomposes into harmless components. Potassium hydroxide (KOH, ACS reagent, ≥85 wt%, Sigma-Aldrich, Ontario, Canada) was used to create the alkaline media for the reaction and adjust the pH during titrations. Sodium hydroxide (ACS reagent, ≥97.0 wt%, pellets) and hydrochloric acid (37 wt%) were both obtained from Sigma-Aldrich (Ontario, Canada); the latter was employed to separate humic acids from fulvic acids. Additionally, potassium bromide (KBr, Sigma-Aldrich, Ontario, Canada) was used in the FTIR analysis.

2.2. Sonoreactor setup and procedure

The chemical reaction was performed in a stainless steel ultrasonic reactor with a maximum capacity of 65 mL and a wall rated for a maximum pressure of 690 kPa. The reactor, equipped with a high-frequency transducer, converts electrical energy into mechanical vibrations, creating ultrasonic waves that promote cavitation, micro-jets, and acoustic streaming within the reaction mixture, as shown schematically in Fig. 1. Reactants, including LRC, water, KOH, and H_2O_2 were added to the reactor vessel (this is considered time zero in the reaction). Then the vessel was tightly closed, and the ultrasonic waves started to create micro-jets and micro-streams in the liquid, promoting mixing and enhancing mass transfer.[26] Additionally, the cavitation bubbles produced by the ultrasonic waves help break down larger LRC particles into smaller ones, further increasing the surface area of the reactants and making them more accessible to each other.[27]

Reaction parameters, including reaction time, amplitude, and ultrasonic pulsing, were controlled using the control panel. Higher amplitudes were avoided to reduce energy consumption, prevent tip degradation, and prevent the generation of elevated temperatures. Temperatures were monitored during reactions using a thermocouple inserted at the bottom of the reactor. A pressure gauge was used to monitor pressure buildup, and gas samples were collected using double-ended sample cylinder fitted with pressure gauges (Swagelok, Canada) for gas chromatography (GC) analysis. Upon completion of the reaction, the reactor is left to cool down, gas samples were taken from the closed reactor vessel. The produced liquid (*i.e.*, desired products) was collected and centrifuged to remove any suspended and undissolved/unreacted particles and then characterized to quantify the humic and fulvic acid content. Humic acids were separated from fulvic acids based on ISO 19822 standard. The general concept behind the standard is based on acid titration

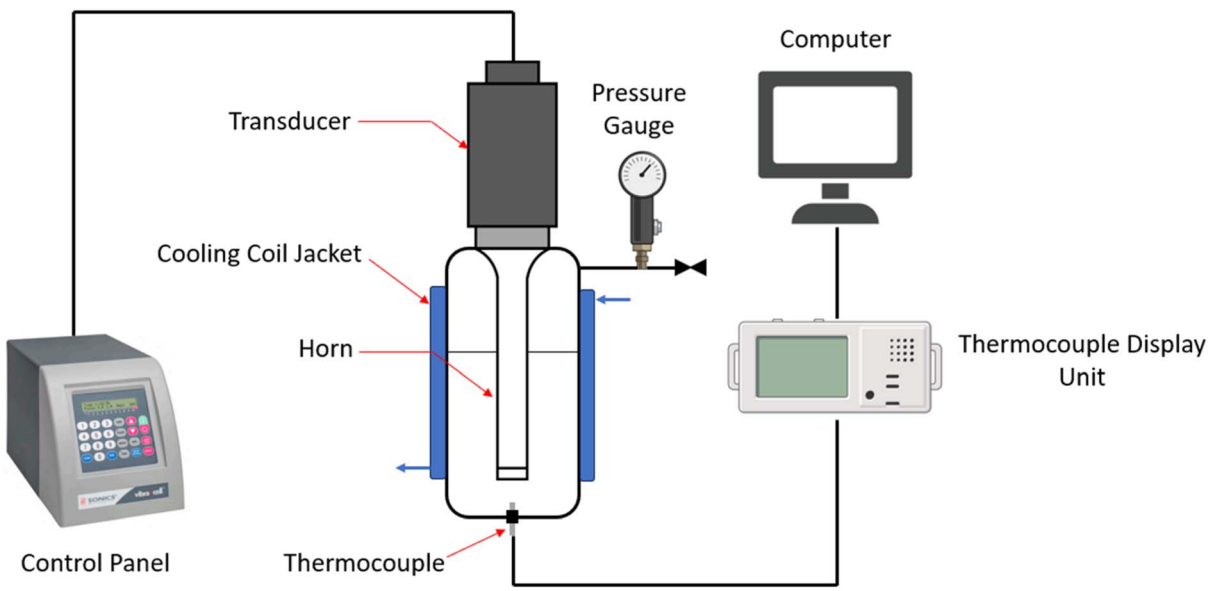

Fig. 1 Illustrative sketch for the ultrasonic reactor unit showing reactor vessel, transducer, cooling jacket, control panel and temperature monitoring setup (not to scale).

to precipitate the humic acids from the solution as the pH of the solution is reduced to 1. The extracted humic fraction is then separated from the solution using centrifugation at 3900×*g* for 30 min.[23] Residual solids (leftover undissolved/unreacted material after centrifugation) were collected, vacuum dried at 65 °C and weighed. A mass balance was performed to account for the distribution across gas, liquid (humic and fulvic acid) and solid residue phases.

2.3. Analytical methods

2.3.1. Potentiometric analysis. Potentiometric analysis was performed on a single sample of liquid humic acids derived from each type of LRC at the optimized conditions. The purpose of this analysis is to quantify the functional groups of phenolic and carboxylic acids. Initially, a standardized solution of 0.1 M HCl was prepared. Subsequently, the liquid humic acid solution was titrated with the HCl solution while monitoring the pH change throughout the process. As HCl was added, the pH of the solution decreased, causing humic acids to precipitate. The precipitated humic acid was collected for further treatment and characterization. The titration endpoint was determined at the inflection point on the titration curve, indicating complete saturation of the acidic functional groups. The inflection point was identified using the derivative of the titration curve, and the volume of HCl at that point was recorded. The total acidity, including both carboxylic and phenolic functional groups, was calculated based on the titration data. The differential method $\Delta pH/\Delta V = f(V_{HCl})$ was used to find the maximum inflection points. The first inflection point is assigned to carboxylic functional group and the second for OH functional groups.

2.3.2. Fourier transform infrared (FTIR). All precipitated humic acid samples were vacuum dried at 65 °C before FTIR analysis. A portion of each dried sample was finely ground and mixed with KBr; a reference material used for FTIR. The prepared mixture was then transferred to the sample holder for analysis. The FTIR spectra were obtained using an IRAffinity-1S (Shimadzu Corporation, Model No. 3116465, Mandel, USA). The spectra range covered from 400 to 4000 cm^{-1} with a resolution of 2 cm^{-1}. To enhance the accuracy and interpretability of the results, normalization and smoothing of the spectra were performed, minimizing noise and allowing for direct comparison between samples.

2.3.3. Proximate and ultimate analysis. Proximate analysis was conducted using a thermogravimetric analyzer (TGA; SDT Q600 TA Instruments, Inc., New Castle, DE) first under a nitrogen (N_2) atmosphere to study mainly pyrolysis (thermal decomposition), followed by an air atmosphere to study oxidation/combustion based on the ASTM E1131-20.[28] TGA was also used to carry out the mass balance calculations by analyzing feedstock, humic acids and fulvic acid analogs under an air atmosphere to determine the moisture and ash content. From these measurements, the values for moisture, volatile matter, fixed carbon, and ash were determined.

For ultimate analysis, a PerkinElmer 2400 Series II CHNS/O Elemental Analyzer (Waltham, Massachusetts, USA) was utilized to quantify the carbon, hydrogen, and nitrogen content in humic acids, fulvic acids, and virgin feedstock samples. Before analysis, all samples were thoroughly dried and homogenized to ensure uniformity. The oxygen content was determined indirectly by subtracting the total percentages of carbon, hydrogen, nitrogen, and ash from 100%. Ratios such as oxygen-to-carbon (O/C), hydrogen-to-carbon (H/C), and oxygen-to-hydrogen (O/H) were subsequently calculated from the elemental composition to provide insights into the structural characteristics of the samples.

2.3.4. ^{1}H nuclear magnetic resonance (^{1}H NMR). The ^{1}H NMR spectrum of the humic acid sample was obtained using a Bruker 600 MHz spectrometer (Avance III, Bruker BioSpin GmbH, Billerica, MA, USA) with a 4 mm BL4 liquid probe. The spectrum acquisition employed an across-polarization program and spin rate of 8 *k* to ensure resolution and spectral clarity. The collected data were analyzed using Mnova NMR software for processing and interpretation.[29] The NMR results provided detailed insights into the hydrogen-containing functional groups within the humic acid structure, complementing the elemental and functional group analyses.

2.3.5. Gas chromatography analysis (GC). After completing the ultrasonication reaction and allowing the system to cool down to room temperature, gas compositional analysis was performed using a GC (SRI 8610C Multiple Gas #5 gas chromatograph SRI Instruments, Torrance, CA) equipped with a thermal conductivity detector (TCD) and flame ionization detector (FID). Each sample was repeated at least three times for reproducibility and accuracy of the measurements, and the standard deviations were calculated and presented in the figures. The data obtained were used for closing the mass balance on the bulk materials (coal, humic acids, fulvic acids and CO_2) and performing the kinetic analysis of the reaction.

2.4. Reaction kinetics modeling

The lumped double triangular kinetic reaction model is proposed here to determine the key kinetic parameters, like rate constants, apparent activation energies, pre-exponential factors, and reaction orders. Fig. 2 shows a schematic diagram of this proposed reaction. This approach simplifies the complex network of reactions by grouping multiple components and elementary reactions into an apparent reaction model to describe the chemical reactions involved in the transformation of LRC into humic acids, fulvic acids, and CO_2.[30] This model utilizes the Arrhenius equation (eqn (1)) to characterize the rate of these reactions based on temperatures and apparent activation energies. The LRC-to-humic substances process is divided into six pathways, each governed by its specific reaction constant (k_i). This allows for the examination of how each reaction pathway contributes to the overall conversion and how temperature influences these contributions. A limitation of this lumped approach is that it simplifies the structural diversity of the reactants and products into single entities. Consequently, the derived kinetic parameters, such as activation energies and rate constants should be interpreted as apparent values that describe the net effect of numerous parallel and sequential reactions, rather than corresponding to distinct mechanistic steps. Despite this, the model remains an invaluable tool for engineering applications, effectively

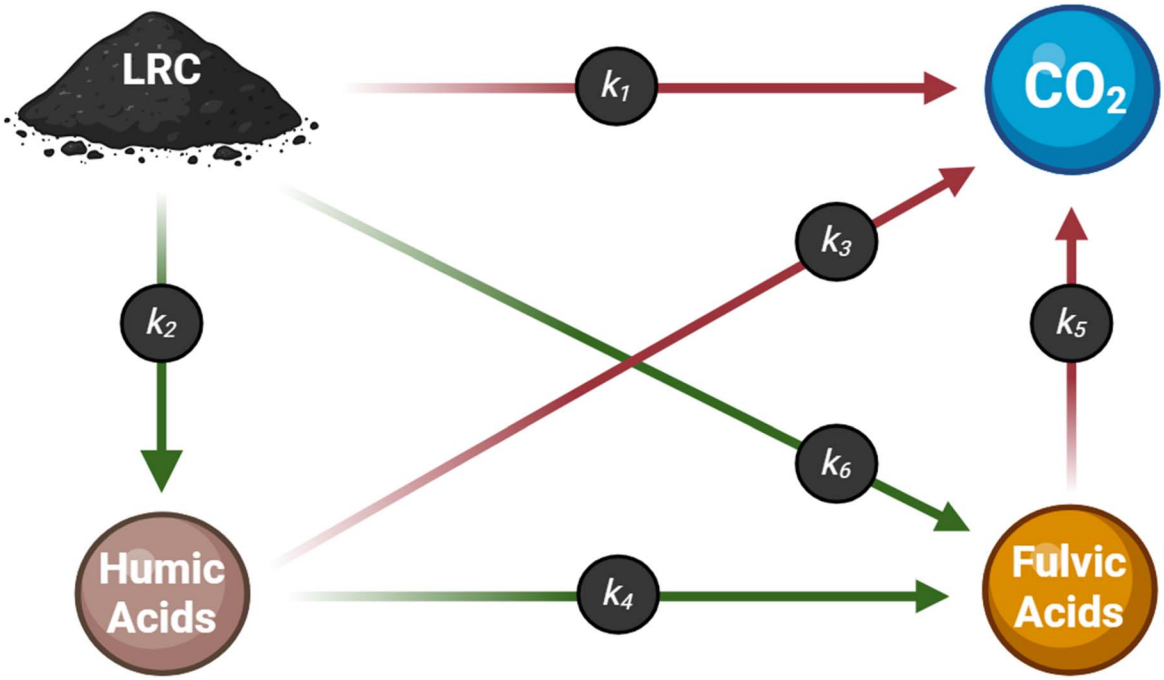

Fig. 2 Schematic representation of the reaction kinetics model proposed for the conversion of LRCs to humic substances.

capturing the macroscopic behavior of the system and enabling process optimization.

The kinetic analysis facilitated by the proposed model is essential for optimizing ultrasonication conditions. By identifying the dominant reaction pathways and their temperature sensitivity, it is possible to fine-tune processing parameters, ensuring maximum yield and efficiency of humic substance production. This approach has been widely applied in chemical and biochemical reaction systems to simplify the analysis of multi-component reactions, as supported by prior studies.[31]

Eqn (1)–(5) show the rate of the reactions for the lumped double triangular kinetics model presented in Fig. 2 along with the Arrhenius equation. These rate equations were used to fit the experimental data by estimating the rate constants (k_1, k_2, k_3, k_4, k_5, k_6). Once the squared errors between calculated values and experimental values were minimized, the rate constants values were used to solve eqn (1) graphically by linearizing the equation first and plotting the natural logarithm of the rate constants against the reciprocal of temperature ($1/T$). The slope of each best-fit-line represents ($-E_a/R$), and the intercept represents ($\ln(A)$).

$$k_i = A_i e^{\frac{-E_{ai}}{RT_i}} \quad (1)$$

$$-r_A = k_1 C_A + k_2 C_A + k_6 C_A \quad (2)$$

$$r_H = k_2 C_A - k_3 C_H - k_4 C_H \quad (3)$$

$$r_F = k_6 C_A + k_4 C_H - k_5 C_F \quad (4)$$

$$r_C = k_1 C_A + k_3 C_H + k_5 C_F \quad (5)$$

where r_A, r_H, r_F and r_C are the reaction rates for the disappearance of LRC and the formation of humic acids, fulvic acids and CO_2, respectively. C_A, C_H, C_F, and C_C are the concentrations of LRC, humic acids, fulvic acids and CO_2, respectively. The term (A, s^{-1}) represents the pre-exponential factor, also known as the frequency factor. A higher value of A typically indicates that the reaction inherently has a higher tendency to occur. The magnitude of the apparent activation energy (E_a, kJ mol^{-1}) can provide insights into the probability of a reaction to occur.

The kinetics model was conducted on the bulk reactants and products based on moisture-free and ash-free basis following this equation:

$$m_{in} = m_{HA} + m_{FA} + m_{CO_2} + m_R + e \quad (6)$$

where m_{in} is the mass of reactants fed into the reactor, m_{HA} is the mass of humic acid produced, m_{FA} is the mass of fulvic acids produced, m_{CO_2} is mass of CO_2 released during the reaction, m_R is the mass of any residual or unreacted material, and e is the error value for closing the mass balance. Concentrations have been calculated based on the following equation:

$$C_{A,HA,FA} = \frac{m_{A,HA,FA} - m_m - m_a}{m_s} \quad (7)$$

where $m_{A,HA,FA}$ is the initial mass of either LRC, humic acids, or fulvic acids obtained through acid treatment separation. m_m is the mass of moisture; m_a is the mass of ash and m_s is the mass of solution.

2.5. Statistical analysis

To ensure reproducibility, all reported values, including conversion, yield, and quality metrics, were derived from at least three independent experiments. The values reported in

text and figures represent the arithmetic mean, and the corresponding error bars indicate the standard deviation of these replicates. The goodness-of-fit for the kinetic model against experimental concentration data was evaluated using the Root Mean Square Error (RMSE). For the linear regression of the Arrhenius plot, the coefficient of determination (R^2) was used to assess the quality of the fit.

3. Results and discussion

3.1. Reaction conversion and yield of humic and fulvic acids

The conversion of LRC samples using ultrasonication process was calculated based on the following equation:

$$\text{Conversion} = \frac{\text{The amount of coal consumed(free ash and moisture)}}{\text{The amount of coal fed to the reactor(free ash and moisture)}} = \frac{m_{\text{LRC}_0} - m_{\text{LRC}}}{m_{\text{LRC}_0}} \times 100\% \quad (8)$$

where m_{LRC_0} is the amount of LRC added to the solution at the beginning of the reaction (free ash and free moisture) and m_{LRC} is the amount of residue of LRC at the end of the reaction (free ash and free moisture). Fig. 3a shows the conversion for the four types of LRCs at different reaction times ranging from 5–40 min, and at fixed operating parameters, such as ultrasonic amplitude, pH of solution, and ratio of LRC to water. As seen, the reaction conversion of all LRCs depends on the reaction time, as evidenced by an increasing trend in conversion with longer sonication. Prolonged ultrasonication physically and chemically affects the LRC molecules, enhancing mixing through microjets and cavitation-induced microbubbles, which promote diffusion and higher reaction rates. Yaralioglu *et al.* observed rapid mixing under similar conditions when introducing phenolphthalein solution and sodium hydroxide dissolved in ethyl alcohol.[32] The formation of microbubbles through cavitation can fracture the particles of the LRC, causing more diffusion and, consequently, higher reaction rates. Ambedkar *et al.* described four stages of particle breakage in an Indian coal, namely surface pitting, crack formation, crack widening, and particle breakage.[33] Chemically, ultrasonication generates hydroxyl radicals (˙OH), which attack the molecules of LRC, causing oxygenation and allowing for the incorporation of oxygen in the molecular structure as hydroxyl (OH) and carboxyl (COOH) groups. Makino *et al.* confirmed the formation of hydroxyl radicals during sonolysis experimentation using spin trapping.[34]

Among the four LRCs, subbituminous coal exhibited the lowest final conversion (79%), while leonardite showed the highest conversion (91%). At the beginning of the reaction, subbituminous coal outperformed other types of LRCs, while peat had the lowest conversion. Over time, the conversion of subbituminous coal plateaued, likely due to its higher aromaticity, which results in fewer aliphatic chains that have favourable attack sites for ˙OH radicals.[35,36] Peat, with its fibrous nature, required extended exposure to ultrasonication time to overcome particle agglomeration, allowing a greater number of particles to participate in the reaction as exposure time increased. In contrast, leonardite and humalite exhibited the highest conversion due to their elevated oxygen content, providing ideal sites for ˙OH radicals generated through ultrasonication to attack. These oxidized LRC molecules, humalite and leonardite, contained reactive sites such as carbonyl (C=O) groups and weakened C–H or C–C bonds, which facilitated hydroxylation.[37] The hydroxylated intermediates formed during the reaction underwent further reactions such as polymerization and condensation, leading to the formation of larger humic

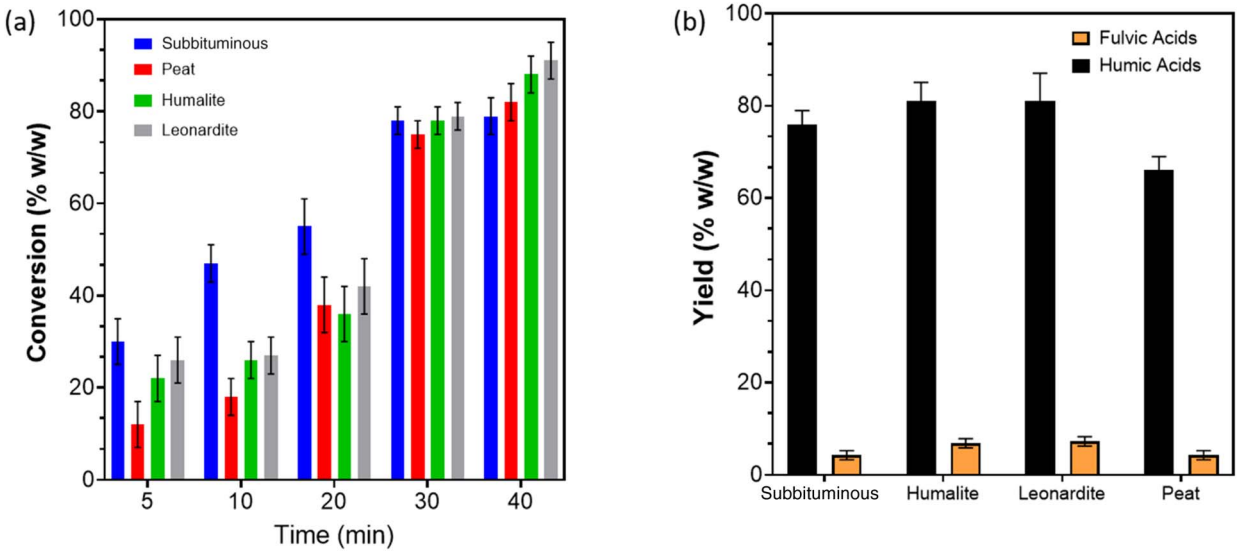

Fig. 3 Conversion of the four types of LRCs across the reaction time (a) and yield of humic and fulvic acids (b) (conditions: 40 min reaction time, 55% amplitude and 3 wt% H_2O_2). Results are shown as mean ± SD ($n = 3$).

acid molecules.[38] The combination of hydroxylation, polymerization, and condensation reactions driven by the reactive intermediates results in a better conversion values for leonardite and humalite.

To further understand the behavior of LRC in the sonoreactor, the yield of humic and fulvic acids at the highest conversion conditions was calculated based on the following equation:

$$\text{Yield} = \frac{\text{The amount of humic or Fulvic acids}}{\text{The amount of LRC in solution}} = \frac{m_{\text{HA/FA}}}{m_{\text{LRC}_0}} \times 100\% \quad (9)$$

where $m_{\text{HA/FA}}$ is the mass of humic or fulvic acids produced (free ash and free moisture) and m_{LRC_0} is the amount of LRC introduced into the reaction. Fig. 3b shows the yield of humic and fulvic acids under fixed conditions, including a reaction time of 40 min, 55% ultrasonic amplitude, pH of the solution, LRC-to-water ratio, and 3 wt% H_2O_2 concentration. Under these conditions, humalite and leonardite achieved the highest yield of humic acids at 81%, while peat had the lowest yield at 66%. Leonardite also exhibited the highest yield of fulvic acid analogs. The high yield of humic acid analogs from leonardite and humalite can be attributed to enhanced mass transfer and improved contact between reactants facilitated by ultrasonic treatment.[39] Compared with previous studies on humic acid production, these findings demonstrate an improvement over conventional technologies in terms of amount of artificial humic acid produced, the reaction time, or both. Sabar *et al.* reported the yield of humic acids of 54.2% and 45.7% generated from subbituminous coal treated with addition of HNO_3 and H_2O_2, respectively, over 11 days of incubation by fungal transformation, compared to 76% for subbituminous coal in this study.[40] Zhu *et al.* achieved a yield of 54% by converting lignite to humic acids using hydrothermal processing at 200 °C.[41] Aftab *et al.* used microwave assisted conversion to achieve ~40% yield of humic acid from low-grade coals.[2] This suggests that ultrasonic irradiation can effectively direct the reaction pathway towards the desired product, by providing the necessary activation energy and breaking down undesired reaction intermediates, as will be elaborated in the kinetics section.[42] The impact of ultrasonic intensification on the conversion and yield of transforming LRC is a significant aspect of this process. Ultrasonic irradiation provides a method of intensifying chemical reactions by generating high shear forces, localized hot spots, and transient cavitation bubbles that result in improved mass transfer, enhanced heat transfer, and mechanical mixing.[42] It is, however, necessary to carefully control the ultrasonic parameters to avoid potential negative effects such as excessive heat generation and undesired side reactions. Another observation from the data reveals that, although subbituminous coal exhibits a lower conversion rate than peat, it contains a higher amount of humic acids, with a calculated yield of 76% compared to 66% for peat. This indicates a greater proportion of reacted peat has been converted to gases, as evidenced by the lower calculated apparent activation energies for CO_2 formation from peat reported in this study. Overall, the ultrasonication of LRC is an effective method to produce humic and fulvic acid analogs at high conversion and yield by improving the mass transfer and increasing the incorporation of oxygen through hydroxyl radical formation.

3.2. Particle size effect

The effect of particle size on humic acid yield was examined for the four types of LRCs considered in this study. Particle size ranges evaluated included >590 μm, 590–425 μm, 425–150 μm, and 150–75 μm. Fig. 4 shows histograms of humic acid yield as function of particle size for each LRC type.

Within the experimental error, the results show that particle size (within the considered range) does not significantly affect the yield of humic acids from leonardite, humalite, and subbituminous coals during ultrasonic processing. However, smaller particle sizes yielded a higher amount of humic acids from peat, likely due to its fibrous structure. This highlights the role of particle size in overcoming mass transfer constraints specific to peat, enhancing the efficiency of ultrasonic processing. In contrast, the absence of significant yield variation with particle size for leonardite, humalite, and subbituminous coals suggests that mass transfer limitations do not play a key role in the ultrasonic conversion process for these materials. Consequently, any of the tested particle sizes can be used effectively for these types of LRC without compromising the yield of humic acids. However, with the traditional humic acid extraction methods, smaller particle sizes have improved the conversion of coals to humic acids. Pájaro-Payares *et al.* showed that finer particle sizes improved the yield of humic acids from Colombian mineral coal through oxidation using $KMnO_4$.[43] Cheng *et al.* found that particle sizes lower than 200 μm improved the yield of humic acids for brown coals using hydrothermal treatment.[13] In this study, ultrasonication facilitated particle fragmentation, as there were no significant differences in the yield across the particle size ranges, except in the case of peat, where its fibrous nature led to variations.[44] This follows our previous observations on the conversion of peat, which require longer ultrasonication times to achieve higher conversion values. Therefore, we recommend either allowing sufficient ultrasonication time for ultrasonic waves to break down the fibrous structure of peat or grinding the samples to a size below 425 μm. Overall, this emphasizes the importance of particle size optimization depending on the LRC type and highlights the impact of ultrasonication on particle fragmentation.

3.3. Effect of KOH concentrations

Although the conversion of LRC can be achieved using other alkalis such as NaOH, high sodium content in humic and fulvic acids has been associated with negative effects on soil health and plant growth.[45] Therefore, here we focus on examining the effect of varying the concentrations of KOH on the conversion of LRC to humic and fulvic acid analogs, as potassium is an essential nutrient for plants and crops, making KOH a more suitable choice for agricultural applications. The potassium ions (K^+) from the KOH neutralize the acidic carboxylic and

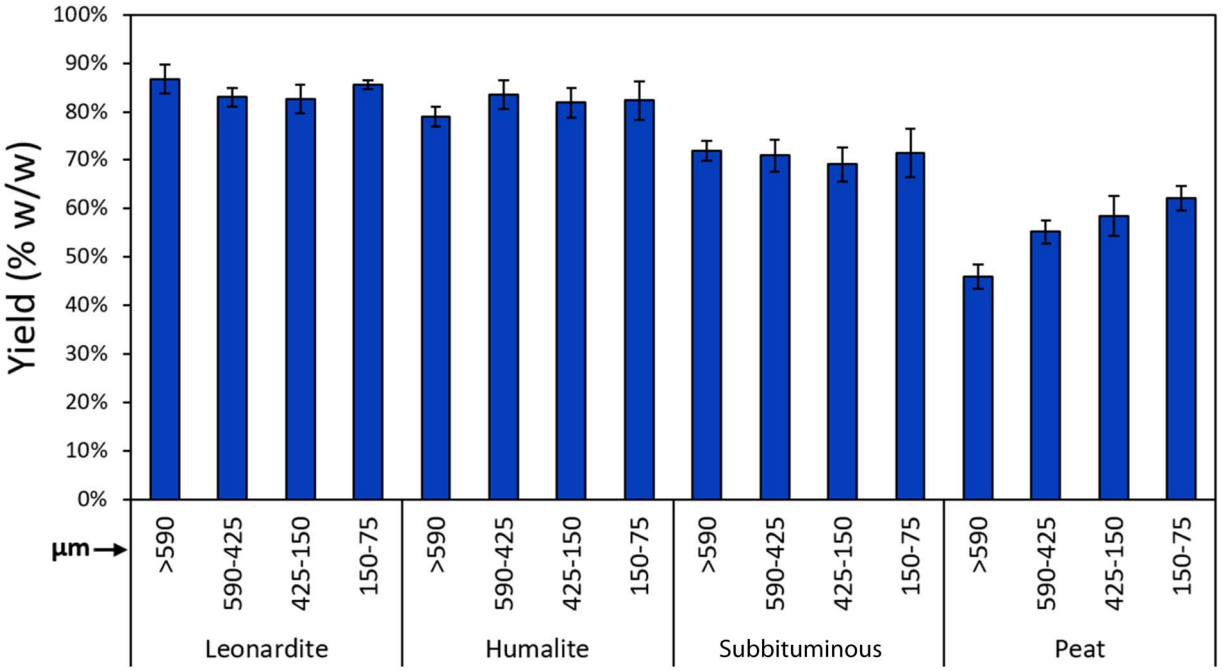

Fig. 4 Particle size effect on the yield of humic acids for four types of LRC (conditions: 40 min reaction time, 55% amplitude and 3 wt% H_2O_2). Results are shown as mean ± SD ($n = 3$).

phenolic functional groups formed on the humic and fulvic acid backbones. Potassium is one of the three essential primary macronutrients for plant growth (the 'K' in N–P–K fertilizers). Fig. 5 shows the effect of three different concentrations of KOH (1.25, 2.5, and 3.75 wt%), at a fixed amount of LRC, on the conversion rates of the four types of LRC. Concentrations exceeding 3.75 wt% were avoided based on our previous findings on lignite, where it was observed that higher concentrations, beyond 3.75%, did not improve conversion.[23] Additionally, higher base concentrations were shown to reduce the yield rates of humic acids due to decreased solubility at high ion strengths, as humic acids behave as colloids.[46,47] As shown, the four types of all four LRC exhibit a consistent increasing trend with higher KOH concentrations. This suggests that the conversion process is strongly influenced by the concentration of the KOH. Huey *et al.* studied the effect of KOH on the conversion of peat to humic acids and showed a similar increasing trend.[48] Li *et al.* also reported similar trends working

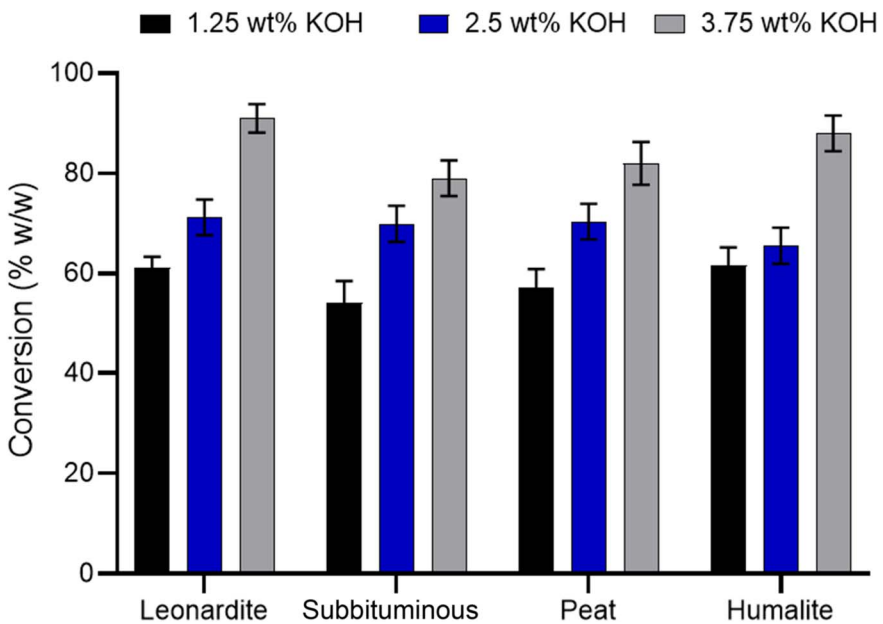

Fig. 5 Effect of KOH concentrations on the conversion for the four types of LRC (conditions: 40 min reaction time, 55% amplitude and 3 wt% H_2O_2). Results are shown as mean ± SD ($n = 3$).

with lignite conversion to humic acids.[49] The roles of KOH in the ultrasonication reaction can be explained across multiple stages. KOH acts as a solubilization agent, aiding in the solubilization of produced humic and fulvic acid analogs. During the reaction, monovalent K^+ ions substitute protons on carboxylic (COOH) and phenolic groups, disrupting hydrophobic and hydrogen bonds and enabling the acids to dissolve as salts (*i.e.*, K-humates).[50] This prevents humic and fulvic acid intermediates from further converting into CO_2, as observed in the kinetics study, where CO_2 forming reactions exhibited the highest activation energies. Furthermore, KOH acts as a catalyst, facilitating the adsorption of hydroxyl ($^{\bullet}OH$) radicals onto LRC molecules, enhancing diffusion, and increasing reaction rates.[51,52] It also participates in reactions such as saponification, further contributing to the conversion process.[53] These roles of KOH, beyond being a simple solubilizing agent, account for variations in trends observed among the four types of LRC.

3.4. Effect of LRC concentrations

Increasing the concentration of LRC in the reaction reduces the water usage and improves the quality of the humic substances produced (defined as the concentration of humic substances in the liquid solution). Experiments were conducted for the four types of LRC at concentrations of 5, 10, and 15 wt% while fixing all other parameters. Fig. 6a shows the effect of LRC concentrations on the reaction conversion at fixed ultrasonication parameters (55% amplitude and 40 min reaction time). As seen, for all the types of LRC, the higher the concentration, the lower the conversion. This trend is attributed to the nature of the chemical reaction involved in LRC conversion, which requires a well-dispersed LRC-water matrix to maximize surface area interaction.[54]

At higher LRC concentrations, issues such as viscosity, solubility, agglomeration and sedimentation increase, constraining the effective surface area available for reactions. Furthermore, acoustic streaming, which is responsible for mixing in the sonoreactor, becomes inefficient as more solids are introduced. Solubility plays an important role, a higher concentration of LRC can lead to a saturation point where these substances exceed their solubility in water, causing precipitation and inhibiting further conversion.[55] Additionally, high LRC concentration could lead to a relative scarcity of essential reacting species, such as $^{\bullet}OH$ radicals, slowing down the conversion rate due to limited availability of these groups. Thus, achieving an optimal balance in LRC concentration is important for efficient conversion into products. These findings align with other studies, such as Rashid *et al.* who showed a reduction of 25–60% in the extraction of humic acids when increasing the concentration of coal due to lower cohesive energy and higher viscosity of the treated mixture.[56] Despite the lower conversion rates, higher concentrations of LRC improve the quality of the humic acid products due to the same water volume being used in all the experiments, but it results in increased unreacted LRC residues (Fig. 6b). For example, at 5 wt% leonardite, a conversion of about 91% corresponds to a quality of about 3.6 wt%, using the ISO 19822 method; while at 15 wt% leonardite, the conversion drops to around 60% but the quality improves to 7.2 wt%.

Consequently, ultrasonication becomes less effective as acoustic streaming, essential for mixing, diminishes with higher solid content. For optimal results, we recommend using 5 wt% LRC to obtain higher conversion rate with minimal residue. However, if solid handling is not a limitation, higher LRC concentrations can be advantageous for achieving improved product quality, as they yield a more concentrated humic acid solution.

3.5. Optimization of sonoreactor parameters

3.5.1. Ultrasonic pulsing. Ultrasonic pulsing involves alternating the ultrasonic energy on and off in either a fixed or random pattern, typically within seconds. This parameter is used to reduce the overall ultrasonic power utilization, reduce heat generation during the reactions, improve reaction rates, and improve the efficiency of ultrasonic waves. Xu *et al.* found that pulsing is effective in increasing the extraction yield of all-trans-lycopene from red grapefruit.[57] Kobus reported that pulsed ultrasound accelerated the extraction of bioactive components from dried roots of valerian compared to

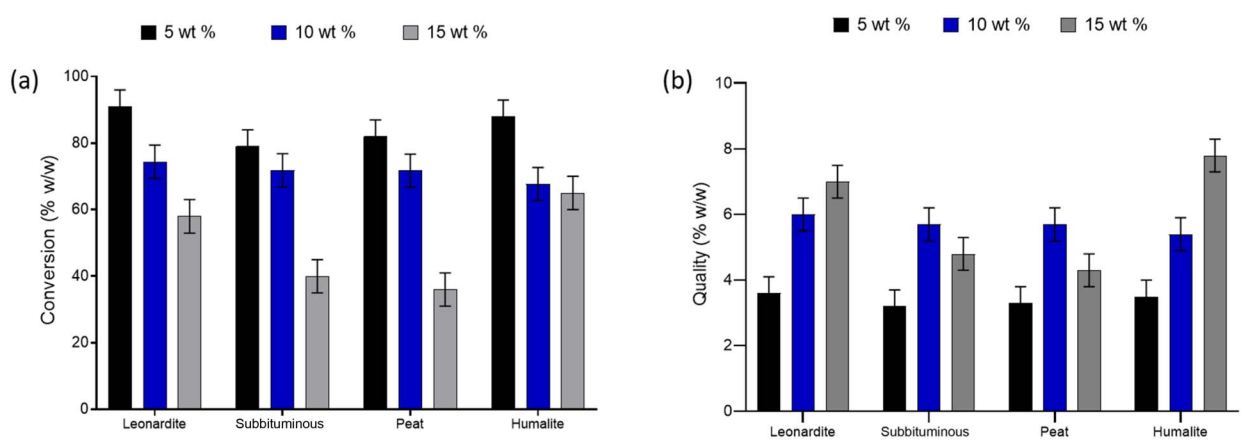

Fig. 6 The effect of LRC concentration on the conversion (a) and quality (b) of humic acids under the optimized conditions (conditions: 40 min reaction time, 55% amplitude and 3 wt% H_2O_2). Results are shown as mean ± SD ($n = 3$).

continuous ultrasound.[58] Similarly, Kadkhodaee *et al.* found that sonication at 50% on and 50% off had a beneficial impact on the extraction process and yield of active compounds from saffron in comparison to continuous sonication.[59] Building on these findings, we tested three fixed patterns of pulsing to evaluate their impact on the conversion of LRC to humic and fulvic acids, aiming to optimize the reaction process and enhance efficiency. Fig. 7 shows the effect of ultrasonic pulsing on the conversion of subbituminous coal and the energy used during the reaction. Increasing the ultrasonic pulsing (time when sonication is on) improves the conversion of LRC. Extending the pulsing time from 5 s on and 1 s off to 15 s on and 1 s off resulted in a 4% increase in the conversion. However, this increase comes at a disadvantage of 30% incremental energy consumption, which diminishes the overall efficiency of the process. Therefore, for optimal conversion of LRC using ultrasonication, shorter pulsing intervals are recommended to balance energy efficiency and conversion performance. The high energy increase could be attributed to the reduction of the effective area for sonochemical reactions due to the development of degassing bubbles in the presence of continuous-wave ultrasound. By employing frequent pulse modulation, the generation of degassing bubbles is reduced during the periods of ultrasound inactivity. This facilitates the clarification of the cavitation zone and amplifies the efficiency of sonochemical reactions.[60,61]

3.5.2. Ultrasonic amplitude. Ultrasonic amplitude determines the energy transferred to the solution during sonication. Fig. 8 shows the effect of varying amplitudes on the reaction conversion. At lower amplitudes, such as 25%, the cavitation effect is weak, resulting in limited microbubble formation. Consequently, the interaction between the ultrasonic waves and the LRC particles is less intense, leading to only a moderate increase in the conversion. As the amplitude increases to 40%, the cavitation effect becomes more pronounced. The higher energy promotes the formation and subsequent collapse of more microbubbles, generating localized elevated temperatures and pressures within the liquid. This environment produces $^{\bullet}OH$ radicals, which drive the conversion process more effectively.[62] These reactive radicals, formed inside the microbubbles or in the thin film separating the microbubbles from the bulk solution, initiate and accelerate chemical reactions, leading to an increase in the rate of conversion by breaking down complex organic structures into simpler forms. At the highest amplitude of 55%, the cavitation reaches its peak intensity. The formation and implosion of microbubbles become extremely intense, creating intense shear forces and localized hotspots within the liquid. This cavitation condition enhances the disintegration of large LRC molecules into smaller fragments and promotes the release of soluble components such as humic and fulvic acid analogs. As a result, conversion increases as more complex structures are converted into soluble forms. Studies have consistently demonstrated the positive impact of amplitude or ultrasonic power on the extraction, treatment, and conversion of various chemicals.[63–66]

In this study, we limited the amplitude to 55% to maintain a less severe process in terms of temperature and pressure. Beyond this point, the temperatures of the sonicated solutions started to increase above 70 °C, and pressure buildup increased inside the reactor, potentially due to the increase in CO_2 concentrations. While ultrasonic amplitude is a key factor to enhance the conversion of LRC to humic and fulvic acid analogs, excessive amplitudes are not recommended as higher amplitudes can lead to a rapid temperature increase, increased CO_2 formation, and accelerated degradation of the ultrasonic horn. This erosion of the probe tip, a known challenge in high-

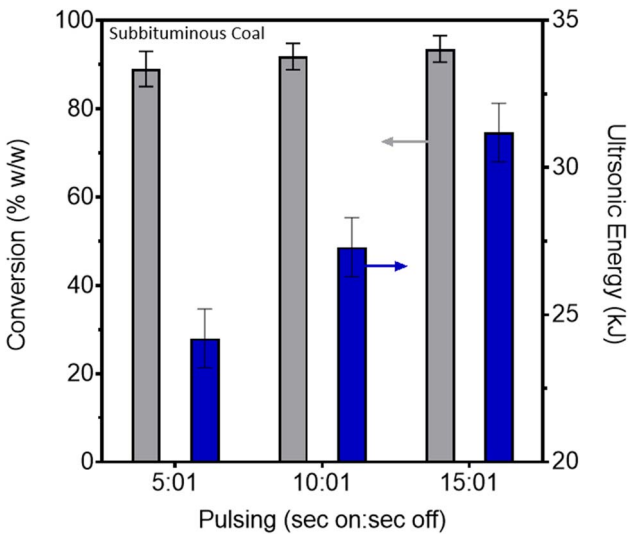

Fig. 7 Ultrasonic pulsing effect on the conversion (grey) for subbituminous coal and ultrasonic energy used during the reaction (blue) (conditions: 40 min reaction time, 55% amplitude and 3 wt% H_2O_2). Results are shown as mean ± SD ($n = 5$).

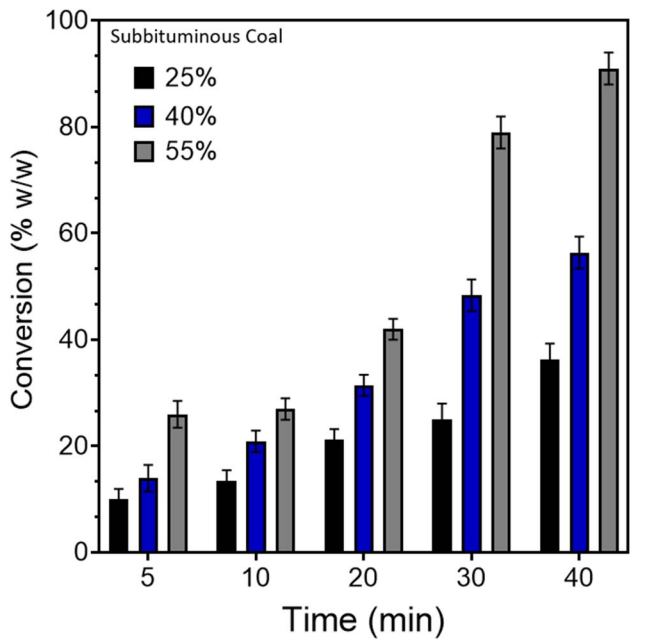

Fig. 8 Effect of ultrasonic amplitude on the conversion of subbituminous coal (conditions: 40 min reaction time, 55% amplitude and 3 wt% H_2O_2). Results are shown as mean ± SD ($n = 3$).

power sonochemistry, represents a significant operational cost and is a primary consideration for industrial scale-up. Therefore, operating at optimized, moderate amplitudes is crucial for ensuring the long-term viability and economic feasibility of the process.

3.5.3. Ultrasonic probe immersion depth. Probe immersion depth refers to the extent to which the ultrasonic probe is submerged into the solution being treated. The longer the immersion depth, the closer the tip of the ultrasonic probe is to the bottom of the reactor vessel. Adjustments were made by repositioning the clamp that holds the horn, ensuring the probe was lowered appropriately. For the reactor vessel, a beaker matching the dimensions of the reactor vessel was used. Fig. 9 shows the conversion of LRC samples at immersion depths of 15, 20, 25, and 30 mm with all other experimental parameters held fixed. As shown, conversion increased as the probe depth was extended. While variables such as amplitude remained unchanged, the solution temperature increased as the probe tip of the ultrasonic approached the vessel's bottom. This temperature increase is likely linked to the transducer's impedance, as Asakura *et al.* observed that changes in liquid height between the transducer and the rigid reflector, inversely impacting the oxidation level.[67]

The enhanced conversion at longer depths can be attributed to multiple factors, including the change of the cavitational activity distribution and the extreme mixing in the liquid phase.[68,69] Klíma *et al.* reported a numerical modeling study that showed probe position influence in ultrasonic cavitational distribution.[70] The results here are in agreement with other studies done on extraction, emulsification, and degradation using sonochemical processes.[69,71,72] The results are significant for the application of ultrasonic treatment in continuous processes. For such operations, positioning the vessel outlet higher to accommodate a deeper probe immersion depth is recommended, as it can enhance conversion efficiency.

3.6. Characterization of products

3.6.1. Fourier transform infrared spectroscopy. Fig. 10 shows four spectra of humic (a) and fulvic (b) acid analogs produced from peat, leonardite, subbituminous coal and humalite. The presented spectra were baseline-corrected prior to analysis. An important finding is the consistency of bands across these spectra, suggesting that humic acid analogs synthesized *via* ultrasonication of LRC exhibit structural similarities in functional group composition. Based on previous studies, there are characteristic bands common to all the spectra of humic acids.[73–77] For example, the broad absorption band centered around 3400 cm^{-1} corresponds to the O–H stretching of phenol and alcohol, visible in all samples.[78] The presence of carboxylic acids represented by carbonyl stretch (C═O) is observed at around 1700 cm^{-1}. A strong band around 1300 cm^{-1} can be attributed to OH and C–O stretching deformation. Other notable bands include the 1500 cm^{-1} band representing CH blending, 1370 cm^{-1} for symmetric blending of CH_3 in CCH_3, and 1000 cm^{-1} for CO stretching in acetate ester. While most of the absorption bands are similar, there are some differences observed. For example, at 2300 cm^{-1}, humic acid analogs produced from peat lack the band seen in the other spectra. This band, attributed to (O═C═O) carbon dioxide, may result from CO_2 adsorption from air during sample preparation. The results suggest that humic acid analogs synthesized from LRC exhibit uniform chemical structures and are not

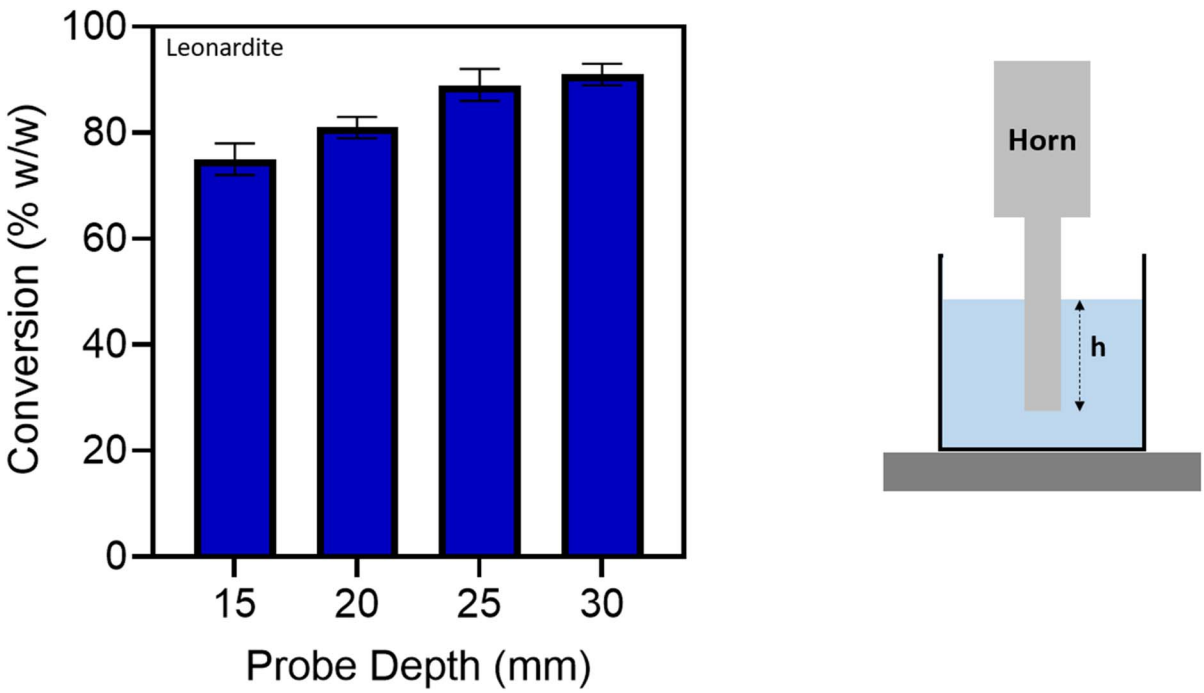

Fig. 9 Reaction conversion for leonardite at different probe immersion depth (h) (conditions: 40 min reaction time, 55% amplitude and 3 wt% H_2O_2). Results are shown as mean ± SD (n = 5).

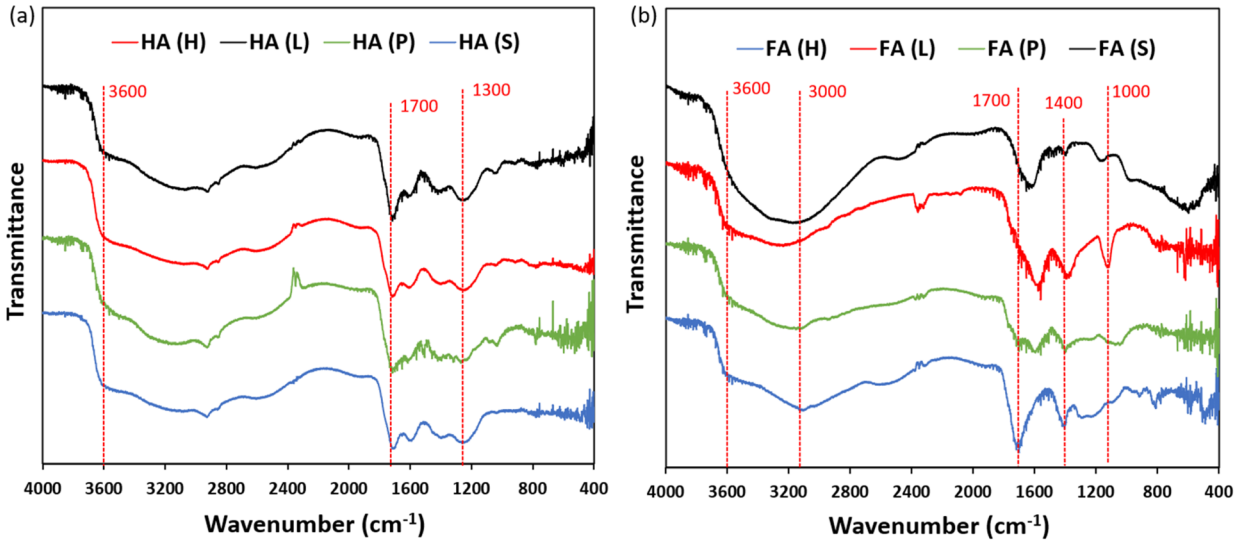

Fig. 10 FTIR spectra showing four samples of humic (HA) (a) and fulvic (FA) (b) acid analogs from four samples of LRC (H: humalite, L: leonardite, P: peat and S: subbituminous).

feedstock-dependent. To quantitatively support this, the intensity ratio of the carboxylic C=O peak to the aromatic C=C peak (A_{1700}/A_{1600}) was calculated, yielding a consistently low value between approximately 0.2 and 0.5 for all humic acid samples. Ultrasonication process effectively achieves higher yields of humic acids within shorter reaction times, without compromising the quality of the resulting humic acids. Along with humic acid spectra, fulvic acid samples generated from four different LRC under identical ultrasonication conditions were analyzed. Despite structural similarities, fulvic acids exhibit notable distinctions from humic acids. Specifically, the presence of stronger carboxylic acid (C=O) signals at 1700 cm^{-1} in fulvic acids suggests higher concentrations of carboxylic functional groups compared to humic acids. This observation is confirmed numerically, as the A_{1700}/A_{1600} intensity ratio for the fulvic acid samples was significantly higher, ranging from approximately 0.8 to 1.1, providing quantitative evidence for a greater degree of oxidation. Fulvic acids derived from leonardite display a prominent band at 1000 cm^{-1}, indicative of CO stretching in acetate esters, while those from humalite exhibit a distinct band around 2500 cm^{-1}, associated with carboxylic acid groups.

3.6.2. Potentiometric titration. Table 1 summarizes the potentiometric titration results for four humic acid samples derived from four LRC types under the same ultrasonication conditions. Across all samples, the carboxylic functional group content is consistently higher than the phenolic functional group. This trend was also confirmed by FTIR analysis. Higher carboxylic groups contribute to enhanced water solubility and improved reactivity with metals and other cations, which is advantageous in various applications.[78,79] Additionally, the total acidity, both carboxylic and phenolic functional groups, is notably higher in humalite and leonardite compared to peat and subbituminous coal. This suggests a higher chelating capacity of humic acids, making these humic acids particularly suitable for agricultural use. These findings align with those reported in the literature, with carboxylic group content ranging from 3 to 7 mmol g^{-1} and phenolic group content between 1 and 5 mmol g^{-1}.[80,81]

3.6.3. Proximate analysis and thermogravimetric analysis. LRCs are characterized by their high moisture and volatile content compared to high-rank coals, presenting distinct thermogravimetric profiles. Thermogravimetric analysis was conducted to evaluate the thermal stability and decomposition characteristics of humalite, leonardite, peat, and subbituminous coals. The results are presented in Fig. 11a. Under inert conditions (nitrogen), samples were heated to 110 °C and held for 5 min to eliminate moisture, and then heated to 950 °C, where they were maintained for 15 min. The gas was then switched to air while the temperature was constant at 950 °C. Under a nitrogen inert environment, the decomposition of the material primarily involves thermal degradation without oxidation, breaking bonds such as C–H, C–C, C–O, and other non-oxidative cleavages. It should be noted that these LRCs typically contain a mix of both aliphatic (C–C and C–H) and aromatic (C=C) carbon bonds, and heteroatomic (C–O, C=O, C–N) bonds, each contributing differently to the thermal behavior.[82–84] The thermal degradation resulted in significant mass loss primarily due to the decomposition of volatile components. Peat exhibited the highest mass loss under nitrogen, followed by leonardite, while subbituminous and humalite coal showed lower losses, indicating higher carbon bond stability in the latter two. Under an air environment, oxidative degradation caused further mass loss, where subbituminous coal showed the highest mass loss, followed by leonardite and humalite, whereas peat displayed the least mass loss. Under an air environment, the breaking of C–H, C–C, C–O bonds occurs alongside the formation of C=O, CO_2, and H_2O. The order of mass loss reflects the sensitivity of the materials to oxidation and oxygenation reactions, with subbituminous coal being the most sensitive due to its high carbon and volatile content. The results highlight the complexity between thermal

Table 1 Potentiometric titration of four humic acid samples obtained from different types of LRC

Sample name	COOH, mmol g^{-1}	OH, mmol g^{-1}	Total acidity, mmol g^{-1}
Humic acid peat	5.4	3.2	8.6
Humic acid humalite	6.3	4.5	10.8
Humic acid leonardite	5.5	4.2	9.7
Humic acid subbituminous	4.4	3.8	8.2

degradation and oxidative reactions, leading to differing behaviors in inert against oxidative environments.

The region up to 200 °C is typically attributed to the release of inherent moisture and some light volatile components. This phase is primarily associated with the breaking of weaker non-covalent interactions rather than the cleavage of specific chemical bonds. The temperature region of 300–500 °C corresponds to the pyrolysis of the LRC, involving the breakdown of aliphatic carbon bonds and the release of volatile compounds not previously released. More stable aromatic carbon structures and other thermally resistant organic components decompose between 500 and 800 °C. Although peat, subbituminous coal, leonardite, and humalite are all classified as LRCs, the TGA curves reveal differences in their chemical structures. These differences influence their distinct behaviors under ultrasonication, as evidenced in the conversion and yield of humic acids from these LRCs. Fig. 11b shows the TAG profiles for humic acid analogs produced from four LRC samples at the same ultrasonic conditions (55% amplitude and 40 min reaction time). As seen, the TGA profile shows four main stages of mass loss occurring at different temperatures. The first stage is characterized by moisture loss due to the evaporation of physically bound water or the loss of highly volatile materials. Peat shows a smaller weight loss in this stage due to its lower moisture content, while subbituminous and leonardite humic acids show the same loss. Humalite humic acids, on the other hand, display the highest loss. This trend may be attributed to the organic matter composition and the maturity of the LRC types. The four types of LRC contain various and types of organic matter, leading to variation in humic acid analog structure and behaviour, as is evident through the various characterization techniques shown in this study. Additionally, the maturity or rank of the coal can influence the volatile materials content in the humic acids. This observation also provides insight into the water adsorption capacity of humic acids derived from these four types. In agriculture applications, humic acids play an important role in improving water retention, enhancing aeration, and facilitating root penetration, thereby promoting better plant growth.[85]

The second stage represents the loss and evaporation of volatile components, along with the breakdown of weakly bonded organic compounds, including aliphatic chains, carbohydrates, and initial aromatic structure degradation. This stage is similar among the four samples of humic acid analogs. The third stage shows the further degradation of aromatic structures and the formation of char. Peat's humic acids show the highest loss in this stage, which can be explained by the immaturity of peat compared to other feedstocks such as humalite, leonardite and subbituminous.[86] The less mature nature of peat may result in a more complex and heterogeneous composition, leading to higher weight loss during thermal decomposition.[87] It may also be an indication of a higher content of functional groups, such as hydroxyl, carboxyl, and phenolic groups. The final stage represents mass loss under air at 950 °C, where any residual carbon or char undergoes oxidation, leading to the formation of CO_2 and other oxidation

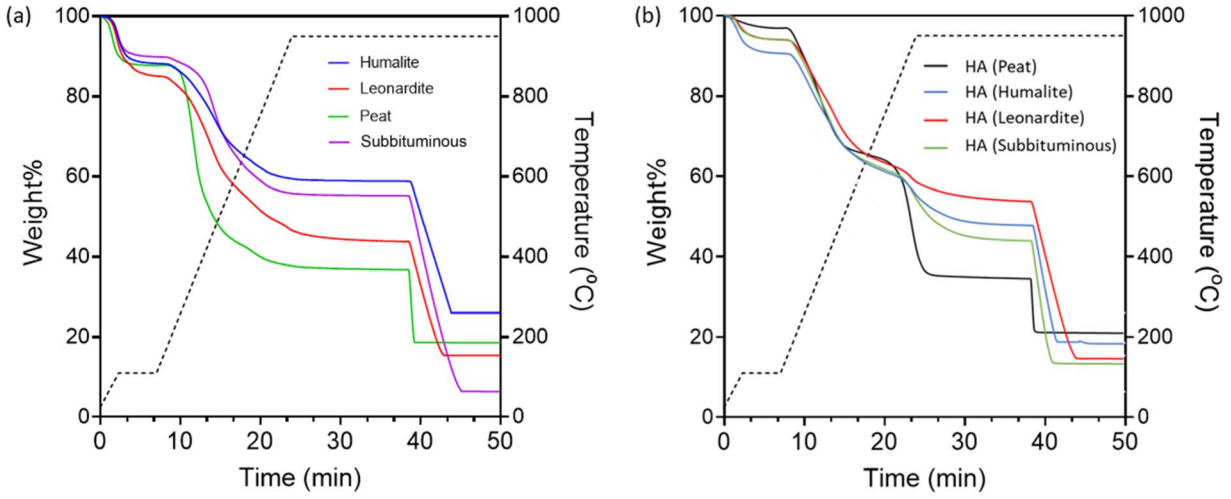

Fig. 11 TGA profiles of humic acids (HA) (b) samples produced from low rank coals (a). TGA was conducted following the ASTM E1131-20.[28] The dotted lines represent the temperature profiles.

products. This stage is most pronounced for subbituminous humic acids, while peat shows the least loss. Humalite and leonardite show similar trends at this stage. The humic acids produced from subbituminous coal may contain more aromatic and condensed structures, which are more resistant to decomposition at lower temperatures, leading to higher weight loss during this stage. Overall, TGA results show similarities and differences in the humic acids formed from the four types of LRC considered in this work, as the maturity and complexity of the source can play a factor in the final product. Table 2 summarizes the values of moisture, volatile matter, fixed carbon, and ash obtained from the TGA curves for all the four types of LRCs and humic acid analog samples.

3.6.4. Ultimate analysis. Table 3 shows the ultimate analysis of virgin LRC samples along with humic and fulvic acid analogs. The oxygen percentage was calculated by the difference between the percentages of carbon, hydrogen, nitrogen, and ash (derived from proximate analysis). Ratios of O/C, H/C, and O/H were calculated on a mass basis. As shown, subbituminous coal exhibits the highest carbon content among the four types of LRC, highlighting its maturity compared to the rest. Conversely, hydrogen content remains similar across all the virgin samples. Nitrogen levels are below 1% in all the four LRC. Leonardite and humalite have higher oxygen content than other feedstocks, as these are oxygenated LRC. The oxygen content in humic and fulvic acids is higher than the virgin sample for all LRC. This observation confirms the incorporation of oxygen through ultrasonication. Another observation is that the oxygen content in fulvic acids consistently exceeds that in humic acids, attributed to the higher prevalence of oxygenated functional groups in fulvic acids. This characteristic contributes to the enhanced ability of fulvic acids to solubilize over a wider range of pH. The degree of oxygenation, reflected by higher O/C ratios, is higher in humic and fulvic acid samples, with humalite-derived humic and fulvic acids showing the most pronounced oxygenation. This can be explained by their high oxygen content and low carbon content compared to other feedstocks. The H/C ratio reflects the aromaticity, does not exhibit a clear trend, indicating that ultrasonication of LRC does not directly break aromatic rings in the virgin LRC. Instead, it attacks aliphatic branches, facilitating the formation of carboxylic and phenolic functional groups.[88] Similarly, the O/H ratio mirrors the O/C trend, reconfirming the higher degree of oxygen incorporation onto humic and fulvic acid analogs. Moreover, humic acids produced from humalite exhibit the highest O/C ratios, suggesting a greater prevalence of O-alkyl and carboxylic acid groups. This correlation is supported by the findings of potentiometric titration. Overall, the elemental analysis confirms the successful incorporation of oxygen into the structure of LRC and the conversion of aliphatic chains to carboxylic and phenolic functional groups.

3.6.5. Proton nuclear magnetic resonance. Using insights from previous studies on humic acid NMR spectra, the ^{1}H NMR was interpreted.[89–91] The ^{1}H NMR spectrum, as depicted in Fig. 12, reveals the presence of aliphatic entities, reflected in chemical shifts ranging between 0 and 3 ppm. The peak at 1.8 ppm typically corresponds to protons in the α-position to carbonyl groups, such as –CH_3 in acetyl groups or –CH_2– in alkyl chains adjacent to carbonyl groups. At 2.4 ppm, the signal corresponds to protons on carbon atoms adjacent to carbonyl groups, such as in acetyl (CH_3–CO–) or methylene (–CH_2–) groups near carbonyls. Peak at 2.6 ppm can be associated with protons in the β-position to aromatic rings or carbonyl groups, for example,

Table 2 Proximate analysis for LRC and humic acid samples (VM: volatile matter, FC: fixed carbon)

		Proximate analysis (%)			
LRC type	Sample	Moisture	VM	FC	Ash
Subbituminous	Virgin	10	35	47	8
	Humic acid	5	52	33	10
Peat	Virgin	12	50	18	20
	Humic acid	2	63	14	21
Leonardite	Virgin	15	43	26	16
	Humic acid	5	40	37	18
Humalite	Virgin	12	28	34	26
	Humic acid	10	45	24	21

Table 3 Ultimate analysis of virgin LRC, the produced humic acids, and fulvic acids samples[a]

		Elemental analysis				Mass ratios		
LRC type	Sample	%C	%H	%N	%O*	O/C*	H/C*	O/H*
Sub-bituminous	Virgin	49.2	4.4	0.98	37.4	0.76	0.09	8.5
	Humic acid	43.6	3.7	0.81	41.7	0.96	0.09	11.2
	Fulvic acid	45.2	4.3	0.51	45.8	1.01	0.10	10.6
Peat	Virgin	45.3	4.7	0.47	29.1	0.64	0.10	6.1
	Humic acid	42.3	5	0.41	31.3	0.74	0.12	6.2
	Fulvic acid	43.3	5.3	0.31	45.9	1.06	0.12	8.6
Leonardite	Virgin	36.8	4.9	0.73	40.8	1.11	0.13	8.2
	Humic acid	35.4	4.3	0.52	41.7	1.18	0.12	9.6
	Fulvic acid	35.2	4.2	0.62	54.2	1.19	0.12	9.96
Humalite	Virgin	29.8	4.4	0.74	38.9	1.31	0.15	8.9
	Humic acid	29.3	3.1	0.66	44.9	1.53	0.11	14.5
	Fulvic acid	25.2	3.5	0.52	66.9	1.61	0.14	12.85

[a] *Calculated values.

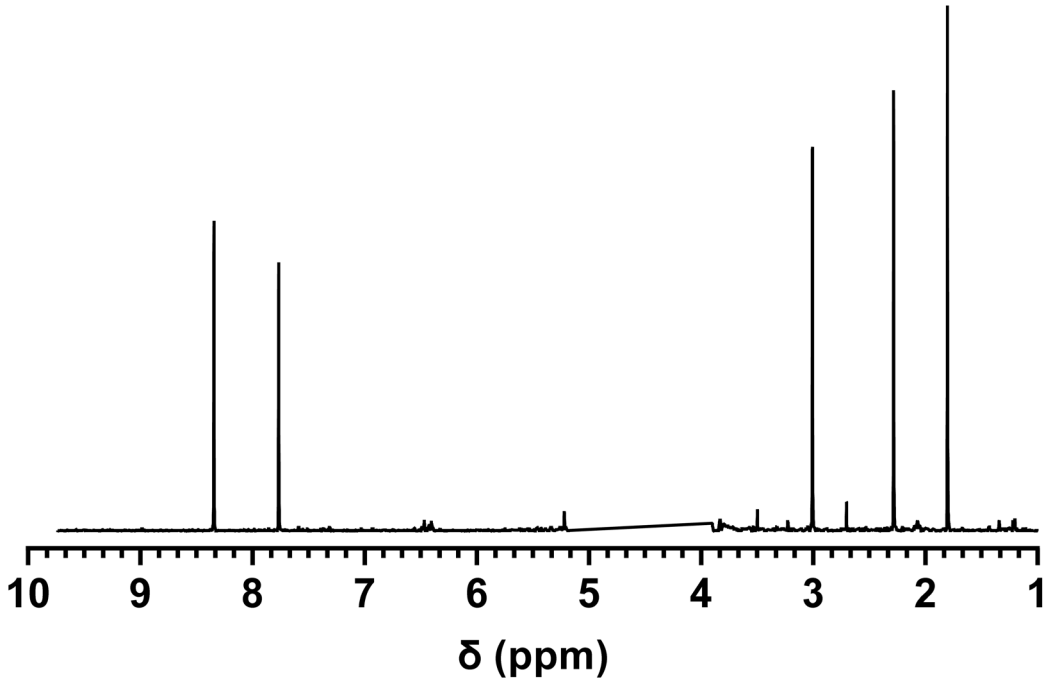

Fig. 12 ^{1}H-NMR spectra for leonardite-derived humic acids sample at the optimized conditions (40 min reaction time, 55% amplitude and 3 wt% H_2O_2).

–CH_2– in phenylacetic acid derivatives or aliphatic chains. The signal at 3 ppm indicates protons on carbon atoms adjacent to electronegative atoms like oxygen or nitrogen, as in –CH_2–OH or –CH_2–NH_2. The small signal at 3.5 ppm reflects protons on carbon atoms bonded to oxygen atoms in alcohols or ethers. A weak signal at 5.2 ppm is associated with vinylic protons (*e.g.*, = CH– in alkenes) or protons in hydroxyl groups of alcohols (OH). The peak at 7.8 ppm is typical for aromatic protons in electron-withdrawing or deshielded environments, influenced by adjacent functional groups. Lastly, the 8.4 ppm signal is characteristic of highly deshielded protons, such as aromatic protons adjacent to strongly electron-withdrawing groups like aldehydes and formyl groups. These observations suggest that during the humification process, carboxyl derivatives and oxygen-bearing hydrocarbons are the predominant water-solubilized fractions. This aligns with our FTIR spectroscopy results and with prior research conducted on humic acid characterization.[92,93]

3.7. Reaction kinetics

3.7.1. Mathematical modeling. The reaction initiates with the breakdown of the complex LRC structure. During this stage, the high-molecular-weight LRC structure is converted into soluble organic compounds, primarily humic and fulvic acid analogs. This conversion is achieved by exposure to oxidizing agents such as hydrogen peroxide. Following the initial conversion into humic acids, further degradation often occurs chemically, resulting in the formation of fulvic acid analogs. These compounds have lower molecular weight and higher solubility than humic acids. Fulvic acids have a greater abundance of carboxyl and hydroxyl functional groups, as reflected in their higher O/C and O/H ratios compared to humic acids, as was shown previously. This degradation also results in the release of CO_2, a byproduct of ultrasonication. Further degradation of fulvic acids may lead to the release of CO_2, completing the transformation of LRC into simpler substances. The concentration profiles for leonardite, shown in Fig. 13, were calculated based on bulk materials after eliminating moisture and ash. Concentration profiles for subbituminous coal, humalite and peat are provided in the SI Materials (Fig. S1–S3).

Mass balance was conducted based on the concentration of LRC introduced into the reactor and the amount of products formed in liquid, solid and gas. Once the mass balance was completed, the concentrations of LRC (C_A), humic acids (C_H), fulvic acids (C_F), and CO_2 (C_C) were plotted over time for three reaction temperatures. Dashed lines in Fig. 13 show the mathematical model fit of the rate equations (eqn (2)–(5)) to the concentration profiles obtained from the experiments. The squares of the errors were minimized, and rate constants (k_i) were obtained. The goodness-of-fit for the model was evaluated by calculating the Root Mean Square Error (RMSE) between the experimental and predicted concentrations, with values ranging from 0.27 to 2.70 across all components and conditions. Using Arrhenius equation, the apparent activation energies (E_a) and pre-exponential factors (A) were calculated graphically. The quality of the linear regression for the Arrhenius plots was confirmed using the coefficient of determination (R^2), with all values falling between 0.9727 and 0.9985, indicating a strong linear fit. For the four types of LRC studied, at higher amplitude, corresponding to higher average temperature, the formation of humic acids is higher, and the rate of disappearance of LRC is also higher. This agrees with our findings from conversion and yield calculations. Another observation is the lower amount of

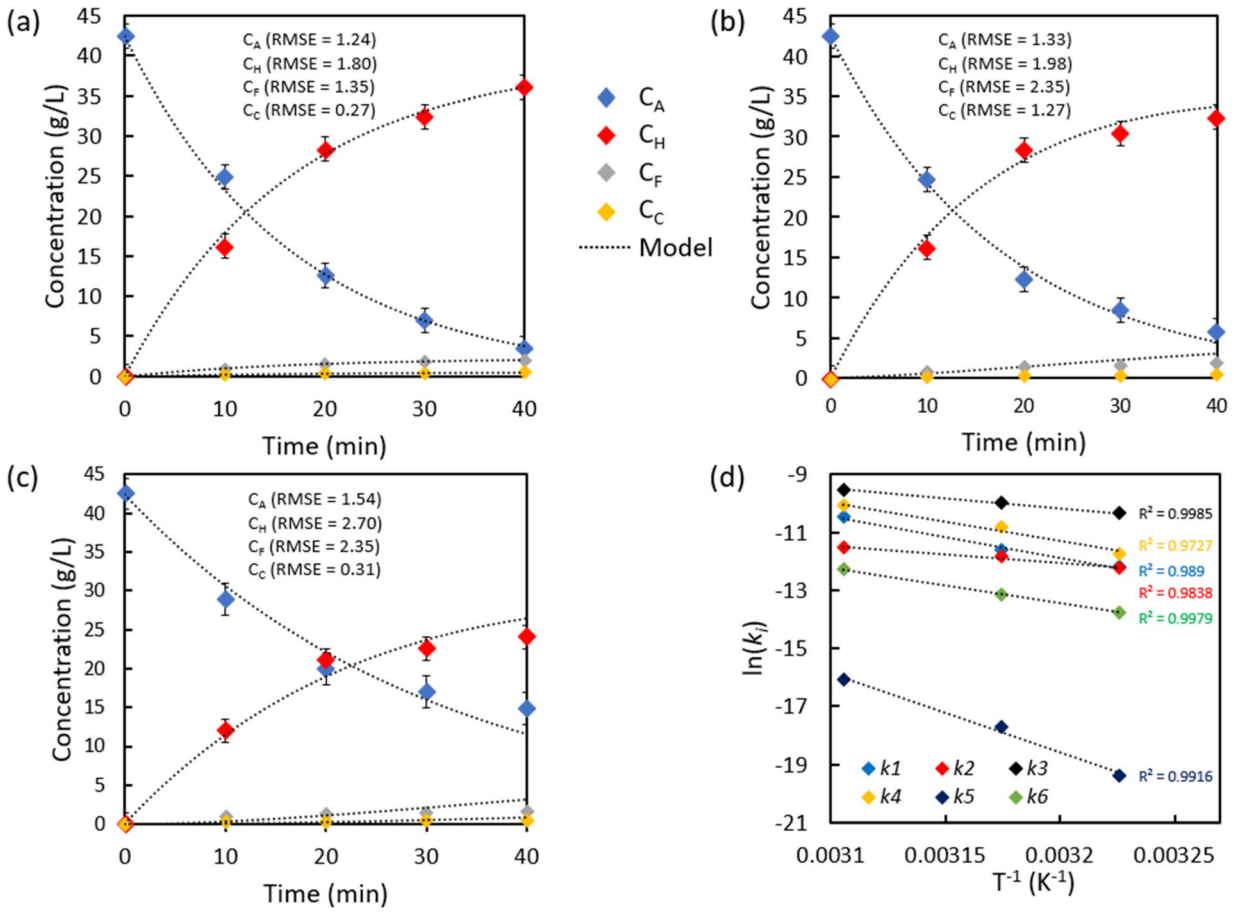

Fig. 13 Concentration profiles showing concentration of leonardite (C_A), concentration of humic acids (C_H), concentration of fulvic acid (C_F) and concentration of CO_2 (C_C). (a) 55% amplitude (b) 40% amplitude and (c) 25% amplitude (d) Arrhenius plot.

CO_2 produced during the reaction at high and lower amplitudes for all LRC types. In stark contrast to direct combustion, which releases 2.4–2.8 kg of CO_2 per kilogram of bituminous coal, our ultrasonic conversion process generates minimal direct emissions, averaging only 0.03 kg of CO_2 per kilogram of feedstock. Crucially, as the process relies on electricity, its overall carbon footprint can be rendered negligible by sourcing power from renewable or other carbon-free energy sources.[1] Furthermore, the production of fulvic acids does not significantly change by changing the amplitude. Table 4 presents the kinetics data for the six reaction pathways involving for four types of LRC, obtained based on the model presented in Fig. 2. The conversion pathways of LRC, humic acid and fulvic acid to CO_2 (Reaction 1, 3, and 5) exhibit higher apparent activation energies compared to other reaction pathways. This indicates that the formation of CO_2 is the least favourable reaction pathway, as also evident in the low concentrations obtained after the ultrasonication. On the other hand, the formation of humic acids (Reaction 2) emerges as the most favourable pathway, with the lowest apparent activation energy among the six pathways. Specifically, the formation of humic acids requires lower activation energy for leonardite and humalite compared to subbituminous coal and peat. This is likely the result of the oxygenated nature of leonardite and humalite, which makes the incorporation of oxygen during ultrasonication easier. This finding is confirmed with the FTIR, TGA, potentiometric titration, and elemental analysis, presented in earlier sections. This relationship is quantitatively illustrated in Fig. 14, which plots the O/C ratio of the feedstock against both the activation energy and the maximum humic acid yield. A clear inverse correlation is observed between the O/C ratio and the activation energy; humalite, with the highest O/C ratio (1.31), has the lowest activation energy (51 kJ mol^{-1}), while peat, with the lowest O/C ratio (0.64), requires the highest (64 kJ mol^{-1}). Concurrently, a positive correlation exists between the O/C ratio and the maximum yield. These trends provide direct quantitative evidence that a higher density of oxygenated functional groups in the feedstock lowers the kinetic barrier for the reaction and leads to a more efficient conversion.

The pathway with the greatest activation energy is identified as Reaction 5, involving the conversion of fulvic acids to CO_2 across all examined LRCs. This suggests that the ultrasonic reaction conditions may not sufficiently facilitate the conversion of fulvic acids into CO_2. Fulvic acids are characterized by high levels of carboxylic and phenolic functional groups, rendering them more susceptible to reaction with potassium hydroxide (KOH). The interaction with KOH can subsequently serve to shield the molecule from undergoing further degradation into CO_2.

Table 4 Reaction kinetics parameters, frequency factors and apparent activation energies. The uncertainty is reported as the 95% confidence interval (CI)

No.	Reaction	Frequency factor A, s^{-1}	Activation energy E_a, kJ mol^{-1}
1	Subbituminous → CO_2	1.09×10^{12}	112 ± 4
2	Subbituminous → humic acids	5.41×10^{7}	60 ± 2
3	Humic acids → CO_2	5.62×10^{16}	154 ± 6
4	Humic acids → fulvic acids	1.17×10^{12}	84 ± 4
5	Fulvic acids → CO_2	8.47×10^{17}	162 ± 6
6	Subbituminous → fulvic acids	2.72×10^{12}	92 ± 4
1	Leonardite → CO_2	3.22×10^{10}	93 ± 4
2	Leonardite → humic acids	1.32×10^{5}	58 ± 2
3	Humic acids → CO_2	1.40×10^{12}	90 ± 4
4	Humic acids → fulvic acids	8.31×10^{10}	63 ± 2
5	Fulvic acids → CO_2	4.58×10^{15}	98 ± 4
6	Leonardite → fulvic acids	1.62×10^{9}	74 ± 2
1	Humalite → CO_2	1.32×10^{9}	91 ± 4
2	Humalite → humic acids	1.90×10^{5}	51 ± 2
3	Humic acids → CO_2	5.10×10^{9}	55 ± 2
4	Humic acids → fulvic acids	5.11×10^{10}	61 ± 2
5	Fulvic acids → CO_2	7.17×10^{11}	111 ± 4
6	Humalite → fulvic acids	1.83×10^{9}	81 ± 4
1	Peat → CO_2	3.72×10^{11}	112 ± 4
2	Peat → humic acids	2.58×10^{6}	64 ± 2
3	Humic acids → CO_2	1.48×10^{12}	106 ± 4
4	Humic acids → fulvic acids	1.83×10^{13}	72 ± 2
5	Fulvic acids → CO_2	2.58×10^{16}	157 ± 6
6	Peat → fulvic acids	4.62×10^{9}	97 ± 4

The activation energy for LRCs conversion to humic acids ranges from 51 to 64 kJ mol^{-1}, which is lower than that of the 79 kJ mol^{-1} reported in our previous study on the conversion of lignite to humic acids using the same process.[23] This difference is likely attributed to the utilization of bulk concentrations in the current study against carbon-specific concentrations as employed in previous work. Furthermore, lignite, as a more complex and mature type of LRC than the ones utilized in this study, inherently requires higher energies. For example, Manasrah *et al.* reported an activation energy for the conversion of petcoke through the oxycracking reaction to humic acids of 71 kJ mol^{-1}.[73] Another study showed an apparent activation energy of 26.14 kJ mol^{-1} through a water-oxygen system to produce humic acids from lignite.[17] The difference in reported activation energies is due to the different models used, type of feedstock, process operating parameters and chemical reactions involved. In contrast, the formation of fulvic acids requires higher activation energies, compared to the formation of humic acids, ranging from 61 to 91 kJ mol^{-1}. This is due to smaller molecules of fulvic acids and higher oxygenated functional groups, as was confirmed in the characterization section. The structural complexity necessitates more energy to overcome the reaction barrier. It is worth noting that forming fulvic acids by further decomposition of humic acids appears to be energetically more favorable than direct formation from LRCs. This stems from the structural similarities between humic and fulvic acids, both rich in carboxylic and phenolic functional groups, facilitating the conversion process, which makes these products easier to oxygenate than the virgin LRC.[94] In contrast, the robust graphite-like structures present in the original coal matrix require significantly higher energy to decompose into smaller molecules like fulvic acids. The stability and complexity of these graphite-like structures in coal requires substantial energy input to break down, making the direct formation of fulvic acids from LRCs less favorable.

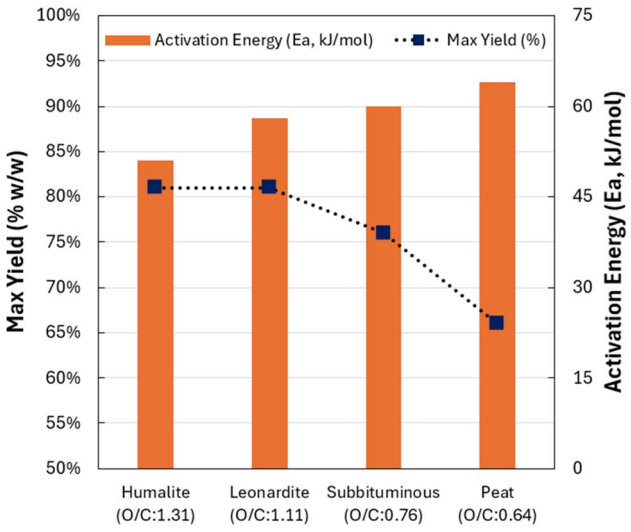

Fig. 14 Influence of feedstock O/C ratio on the apparent activation energy (E_a) and maximum humic acid yield.

For Reaction 1, the apparent activation energies are in the range of 93 and 112 kJ mol^{-1}. Comparatively, Knight *et al.* reported activation energies for LRC to CO_2 through gasification to be 219–233 kJ mol^{-1},[95] while Kwon *et al.* reported a range of 79.07 to 155.64 kJ mol^{-1} for various types of coals.[96] It is critical

to distinguish between the apparent activation energy (E_a), which is the microscopic energy barrier for a reaction (in kJ mol^{-1}), and the macroscopic specific energy consumption (SEC) required to run the entire process (in kJ g^{-1}). In conventional thermal methods, a high activation energy necessitates high operating temperatures, leading directly to high process energy consumption. Our ultrasonication process, however, decouples these factors. By supplying energy *via* acoustic cavitation, it provides a mechanism to overcome the activation energy barrier without requiring high bulk temperatures. This explains how our process can have activation energies in the range of 93–112 kJ mol^{-1} while exhibiting an exceptionally low SEC of a mere 20 kJ per gram of feedstock (0.0056 kWh g^{-1}). This figure is over two orders of magnitude lower than even the most efficient hydrothermal processes reported, which typically range from 0.81 kWh g^{-1} to over 4.0 kWh g^{-1}. This result emphasizes the efficiency and environmental sustainability of the ultrasonic process in producing valuable humic and fulvic acids while minimizing CO_2 emissions, making it a promising alternative to conventional methods.

It should be noted that ultrasound waves at frequencies of 20 kHz (20 000 cycles per second) produce alternating adiabatic compression and rarefaction in the reaction zone. During the rarefaction phase, microbubbles form due to the reduced pressure, a large negative pressure. These microbubbles, typically containing vaporized liquid or gas, grow to a certain size and then explode or implode during the compression cycle. The energy transferred into the liquid through the transducer creates the micro-voids, which, upon collapse, create high local pressures up to 1000 atm and transient temperatures reaching up to 5000 K.[97,98] The phenomenon is called acoustic cavitation or cold boiling.[99]

Table 5 lists several common reactions occurring inside the cavity generated by the ultrasonic energy. The formation of hydroxyl radicals ($^{\bullet}OH$) is caused by the thermal dissociation of water vapor present in the microbubble during the compression phase, as described in eqn (E1). However, additional products such as H_2O_2 and hydrogen gas can also form *via* interactions involving hydroxyl radicals and hydrogen atoms, as shown in eqn (E2), (E4), and (E5). To increase the generation of $^{\bullet}OH$ during the reaction, H_2O_2 was introduced to function as a scavenger of hydrogen atoms, thereby reducing the recombination of $^{\bullet}H$ and $^{\bullet}OH$. Moreover, hydroperoxyl radicals ($HO_2^{\bullet}$), which function as oxidizing agents, are also formed, as represented in eqn (E3). This aligns with previous studies, such as Lin *et al.* who reported that the combination of ultrasound with H_2O_2 increased the efficiency of 2-CPOH decomposition up to 6.6-fold.[100] These results were attributed to the increase of $^{\bullet}OH$ produced by the addition of H_2O_2. Overall, three primary pathways are proposed for the LRC conversion to humic and fulvic acid analogs under sonication. These include oxygen incorporation by hydroxyl radicals, pyrolytic decomposition, and supercritical water oxidation.[101] Hoffmann *et al.* reported that at the layer between the bubble and solution interface, temperature and pressure may reach the critical conditions of water (647 K, 22.1 MPa).[102] They showed that supercritical water is obtained during the collapse of cavitation bubbles generated under ultrasonic treatment. In the interface between the microbubble and bulk liquid, temperatures can reach 2000 K and reactions here are comparable to pyrolysis reactions. Tauber *et al.* found that under ultrasonic energy and low pH, oxidative–pyrolytic reactions predominate for substrates such as 4-nitrophenol, whereas under high pH, $^{\bullet}OH$-radical-induced reactions dominate.[103] In this study, experiments were conducted at higher pH levels, which will result in $^{\bullet}OH$-radical dominating the mechanism of converting LRC to humic and fulvic acid analogs. The attack of $^{\bullet}OH$ radicals facilitate the formation of oxygenated functional groups such as hydroxyl (–OH) and carboxyl (–COOH), as evidenced in FTIR, TGA and ^{1}H NMR, elemental analysis, and potentiometric titration. Once fragmented by ultrasonic energy, the LRC particles undergo decomposition of the unstable oxygenated intermediates, yielding gaseous products and stable complexes functionalized with hydroxyl (phenolic –OH), carbonyl (–CO), and carboxyl (–COOH) groups. Hydroxyl radicals exhibit a pronounced reactivity towards organic substrates, including the molecular structures inherent to LRC. Within the LRC matrix, aliphatic hydrogens attached to sp^3-hybridized carbons are prime targets for radical abstraction. Similarly, hydrogens situated on the periphery of aromatic moieties, characterized by conjugated π-systems, are susceptible to radical attacks. Furthermore, LRC's inherent functional groups, such as hydroxyl (–OH), carbonyl (C═O), and carboxyl (–COOH) moieties, present electrophilic sites conducive for nucleophilic attack by these radicals. Unsaturated loci, delineated by π-bonds in alkenes or alkynes within the LRC structure, also serve as reactive sites for $^{\bullet}OH$ addition. Lastly, bonds associated with heteroatoms like nitrogen, sulphur, and oxygen, embedded within the LRC matrix, may undergo cleavage upon interaction with $^{\bullet}OH$. The subsequent intermediates formed following $^{\bullet}OH$ attack can then participate in an excess of reactive pathways, finishing in an array of products, including CO, CO_2, H_2O, and various oxygenated organic derivatives such as humic and fulvic acid analogs.

Potassium hydroxide plays an important role in the chemical transformation of LRC into humic and fulvic acid analogs. Under alkaline conditions induced by KOH, LRC molecules undergo alkaline hydrolysis, leading to the cleavage of ester and ether linkages. Concurrently, the alkaline conditions induced by KOH promote demethylation and dealkylation processes, facilitating the removal of methyl and other alkyl groups from the aromatic structures inherent to LRC. This demethylation is instrumental in the formation of carboxylic acid groups, a defining feature of humic and fulvic acid analogs.[104] Additionally, the alkaline media encourages the insertion of oxygen into LRC structures, resulting in the creation of phenolic and carboxylic acid groups. Furthermore, KOH enhances the

Table 5 Radical formation and reactions in the sonolysis of water

$H_2O \rightarrow H^{\bullet} + {}^{\bullet}OH$	E1	$^{\bullet}OH + {}^{\bullet}OH \rightarrow H_2O_2$	E5
$H^{\bullet} + H^{\bullet} \rightarrow H_2$	E2	$^{\bullet}OH + {}^{\bullet}OH \rightarrow H_2O + O^{\bullet}$	E6
$H^{\bullet} + O_2 \rightarrow HO_2^{\bullet}$	E3	$^{\bullet}OH + {}^{\bullet}HO_2 \rightarrow H_2O + O_2$	E7
$HO_2^{\bullet} + HO_2^{\bullet} \rightarrow H_2O_2 + O_2$	E4	$O^{\bullet} + O^{\bullet} \rightarrow O_2$	E8

solubility of specific LRC fractions, making them more available to subsequent reactions and facilitating the extraction and isolation of humic acids from the LRC matrix. This was observed by higher activation energies calculated for reactions producing CO_2 from humic and fulvic acids. The inherent acidic functional groups present in LRC are neutralized by KOH, a process that can further steer the reactions in favor of humic substance formation. Through a series of reactive pathways, KOH facilities along with H_2O_2 and $^{\bullet}OH$ radicals the conversion of LRC's complex structure into the more refined and stable humic and fulvic acid analogs. This mechanism highlights the synergistic effects of ultrasonic cavitation and the powerful oxidizing capability of $^{\bullet}OH$ radicals in transforming LRC into humic substances. However, it is worth noting that the exact reaction pathways during this process are likely to be more complex and multifaceted, potentially involving a wide range of intermediates and side reactions.

4. Conclusion

This study highlights the effectiveness of ultrasonic reaction in converting low-rank coals (LRCs), including subbituminous, leonardite, humalite, and peat, into humic and fulvic acid analogs with minimal CO_2 emissions. The optimization of reactant concentrations and sonoreactor parameters reveals relationship of factors governing the reaction conversion. Higher reaction times, amplitudes, and ultrasonic pulsing achieved higher conversions and yields. The important role of amplitude in the ultrasonic reaction is emphasized, with an advisory note against excessive amplitudes due to their potential to produce undesirable CO_2 emissions. Characterization techniques, including FTIR, TGA, elemental analysis, ^{1}H NMR and potentiometric titration, confirmed the formation of humic and fulvic acid analogs with carboxylic and phenolic functional groups. This method represents an advancement over traditional methods of producing humic substances, which often involve higher CO_2 emissions and less efficient processes. The ultrasonic reactor process not only improves yield and product quality but also offers a more environmentally friendly alternative. Kinetic analysis, using the double triangular lump kinetic model, further confirmed that oxygen-rich LRCs, such as humalite and leonardite, are more efficiently converted into humic and fulvic acid analogs. Additionally, reactions forming CO_2 have the highest activation energies, while those forming humic acids have the lowest. This highlights the environmental sustainability of the process, making it a promising technology for large-scale application.

Conflicts of interest

The authors have no competing interests to declare that are relevant to the content of this article.

Data availability

All experimental data supporting the findings of this study are available within the article and its supplementary information (SI). Supplementary information (SI) is available. See DOI: https://doi.org/10.1039/d5su00752f.

Acknowledgements

The authors gratefully acknowledge the Department of Chemical and Petroleum Engineering at the Schulich School of Engineering, University of Calgary. The authors also express their gratitude to Carbon OxyTech Inc., the industrial partner for this research, in collaboration with Mitacs. The authors also extend their appreciation to Alberta Innovates for awarding the Alberta Innovates Graduate Student Scholarship 2024 to the first author, enabling the advancement of this project.

References

1 International Energy Agency, *World Energy Outlook*, Paris, 2024.
2 K. Aftab, J. Javed, U. Habibhah Siddiqua, A. Malik, A. Hassan, M. Rizwan Khan, R. Busquets, N. Ahmad and A. Haque, Process Optimization and Method Validation for Efficient Valorization of Low- Grade Coal into Humic Substances, *Fuel*, 2024, **369**, 131796, DOI: 10.1016/J.FUEL.2024.131796.
3 E. A. Sondreal and G. A. Wiltsee, Low-Rank Coals: Its Present and Future Role in the United States 1, *Ann. Rev. Energy*, 1984, **9**, 473–499.
4 B. Wen, W. Xia and J. M. Sokolovic, Recent Advances in Effective Collectors for Enhancing the Flotation of Low Rank/Oxidized Coals, *Powder Technol*, 2017, **319**, 1–11, DOI: 10.1016/J.POWTEC.2017.06.030.
5 U. Ahmed, M. A. Hussain, M. Bilal, H. Zeb, U. Zahid, S. A. Onaizi and A. G. A. Jameel, Utilization of Low-Rank Coals for Producing Syngas to Meet the Future Energy Needs: Technical and Economic Analysis, *Sustain*, 2021, **13**(19), 10724, DOI: 10.3390/SU131910724.
6 N. S. Akimbekov, I. Digel, K. T. Tastambek, D. K. Sherelkhan, D. B. Jussupova and N. P. Altynbay, Low-Rank Coal as a Source of Humic Substances for Soil Amendment and Fertility Management, *Agric*, 2021, **11**(12), 1261, DOI: 10.3390/AGRICULTURE11121261.
7 G. Lartey-Young and L. Ma, Remediation with Semicoke-Preparation, Characterization, and Adsorption Application, *Mater*, 2020, **13**(19), 4334, DOI: 10.3390/MA13194334.
8 D. Osborne, *The Coal Handbook: towards Cleaner Production*, 2013, Vol. 2, DOI: 10.1533/9781782421177.
9 J. M. K. O'Keefe, A. Bechtel, K. Christanis, S. Dai, W. A. DiMichele, C. F. Eble, J. S. Esterle, M. Mastalerz, A. L. Raymond, B. V. Valentim, N. J. Wagner, C. R. Ward and J. C. Hower, On the Fundamental Difference between Coal Rank and Coal Type, *Int. J. Coal Geol.*, 2013, **118**, 58–87, DOI: 10.1016/j.coal.2013.08.007.
10 I. V. Perminova, F. H. Frimmel, A. V. Kudryavtsev, N. A. Kulikova, G. Abbt-Braun, S. Hesse and V. S. Petrosyan, Molecular Weight Characteristics of Humic Substances from Different Environments as

Determined by Size Exclusion Chromatography and Their Statistical Evaluation, *Environ. Sci. Technol.*, 2003, **37**(11), 2477–2485, DOI: **10.1021/es0258069**.

11 S. V. Eswaran, Value-Added Products From Soil, Brown Coal, and Composted City Solid Waste, *Front. Sustain. Food Syst.*, 2021, **5**, 481, DOI: **10.3389/fsufs.2021.738899**.

12 J. Wu, Y. Zhao, H. Qi, X. Zhao, T. Yang, Y. Du, H. Zhang and Z. Wei, Identifying the Key Factors That Affect the Formation of Humic Substance during Different Materials Composting, *Bioresour. Technol.*, 2017, **244**, 1193–1196, DOI: **10.1016/j.biortech.2017.08.100**.

13 G. Cheng, Z. Niu, C. Zhang, X. Zhang and X. Li, Extraction of Humic Acid from Lignite by KOH-Hydrothermal Method, *Appl. Sci.*, 2019, **9**(7), 1356, DOI: **10.3390/app9071356**.

14 Y. Tang, Y. Yang, D. Cheng, B. Gao, Y. Wan and Y. C. Li, Value-Added Humic Acid Derived from Lignite Using Novel Solid-Phase Activation Process with Pd/CeO 2 Nanocatalyst: A Physiochemical Study, *ACS Sustain. Chem. Eng.*, 2017, **5**(11), 10099–10110, DOI: **10.1021/acssuschemeng.7b02094**.

15 L. Xiao, Y. Li, Y. Liao, H. Ma, J. Wu, Y. Zhang and J. Yao, Bioconversion of Lignite Humic Acid by White-Rot Fungi and Characterization of Products, *3 Biotech*, 2018, **8**(5), 258, DOI: **10.1007/s13205-018-1281-4**.

16 S. S. Fong, L. Seng, N. B. Majri and H. B. Mat, A Comparative Evaluation on the Oxidative Approaches for Extraction of Humic Acids from Low Rank Coal of Mukah, Sarawak, *J. Braz. Chem. Soc.*, 2007, **18**(1), 34–40, DOI: **10.1590/S0103-50532007000100003**.

17 N. Nassar and A. Manasrah, Enhanced Production of Humic Acids from Coal-Lignite *via* Water-Oxygen Systems. *WO2021113978A1*, 2023.

18 Y. Zhang, Y. Li, L. Chang, C. Zi, G. Liang, D. Zhang and Y. Su, A Comparative Study on the Structural Features of Humic Acids Extracted from Lignites Using Comprehensive Spectral Analyses, *RSC Adv.*, 2020, **10**, 19813–19823, DOI: **10.1039/d0ra03166f**.

19 J. Peuravuori, P. Žbánková and K. Pihlaja, Aspects of Structural Features in Lignite and Lignite Humic Acids, *Fuel Process. Technol.*, 2006, **87**(9), 829–839, DOI: **10.1016/J.FUPROC.2006.05.003**.

20 D. Zingaretti, A. Lieto, F. Lombardi and R. Gavasci, Humic Substances Extracted from a Bio-Stabilized Waste Applying Different Operating Conditions, *Waste and Biomass Valorization*, 2020, **11**(10), 5283–5293, DOI: **10.1007/S12649-020-01085-3/TABLES/4**.

21 S. K. Chandra and W. D. Smith, Biological production of humic acid and clean fuels from coal, *US. Pat.*, US5670345A, 1997.

22 N. Nassar; A. Manasrah and R. Al-Akbari, Ultrasonic Reaction for High-Yield Production of Humic Acids from Coal-Lignite, Oxidized Coals, and Residual Feedstocks. *WO 2023/010210 A1*, 2023.

23 R. Al-Akbari, A. D. Manasrah and N. N. Nassar, Production of Humic and Fulvic Acid Analogs through the Ultrasonication of Low-Rank Lignite Coals, *React. Chem. Eng.*, 2024, **9**(3), 566–582, DOI: **10.1039/D3RE00422H**.

24 M. H. Islam and B. G. Pollet, Acoustic Cavitation and Sonochemistry in Industry: State of the Art, *Energy Asp. Acoust. Cavitation Sonochemistry*, 2022, 265–279, DOI: **10.1016/B978-0-323-91937-1.00001-3**.

25 A. Weissler, Formation of Hydrogen Peroxide by Ultrasonic Waves: Free Radicals, *J. Am. Chem. Soc.*, 1959, **81**(5), 1077–1081, DOI: **10.1021/ja01514a015**.

26 F. J. Keil, Modeling of Process Intensification, *Model. Process Intensif*, 2007, 1–405, DOI: **10.1002/9783527610600**.

27 C. Wyatt Shields, D. F. Cruz, K. A. Ohiri, B. B. Yellen and G. P. Lopez, Fabrication and Operation of Acoustofluidic Devices Supporting Bulk Acoustic Standing Waves for Sheathless Focusing of Particles, *J. Visualized Exp.*, 2016, (109), e53861, DOI: **10.3791/53861**.

28 ASTM International, *Standard Test Method for Compositional Analysis by Thermogravimetry (ASTM E1131-20)*, ASTM International, West Conshohocken, PA, 2020, DOI: **10.1520/E1131-20**.

29 MESTRELAB RESEARCH, *Mnova. Mestrelab Research*, 2023.

30 L. Li, P. Chen and E. F. Gloyna, Generalized Kinetic Model for Wet Oxidation of Organic Compounds, *AIChE J.*, 1991, **37**(11), 1687–1697, DOI: **10.1002/AIC.690371112/FORMAT/PDF**.

31 A. D. Manasrah and N. N. Nassar, Oxy-Cracking Technique for Producing Non-Combustion Products from Residual Feedstocks and Cleaning up Wastewater, *Appl. Energy*, 2020, **280**, 115890, DOI: **10.1016/J.APENERGY.2020.115890**.

32 G. G. Yaralioglu, I. O. Wygant, T. C. Marentis and B. T. Khuri-Yakub, Ultrasonic mixing in microfluidic channels using integrated transducers, *Analyst*, 2004, **76**, 3694–3698, DOI: **10.1021/ac035220k**.

33 B. Ambedkar, R. Nagarajan and S. Jayanti, Investigation of High-Frequency, High-Intensity Ultrasonics for Size Reduction and Washing of Coal in Aqueous Medium, *Ind. Eng. Chem. Res.*, 2011, **50**(23), 13210–13219, DOI: **10.1021/IE200222W**.

34 K. Maklno, M. M. Mossoba and P. Rlesz, Chemical Effects of Ultrasound on Aqueous Solutions. Formation of Hydroxyl Radicals and Hydrogen Atoms, *J. Phys. Chem*, 1983, **87**, 1369–1377.

35 P. Zhang, L. Li and C. Ye, Study Of Structural Feature Of Peat, Lignite And Humic Acid By Solid State L3 C NMR Spectroscopy, *Fuel Sci. Technol. Int.*, 1994, **12**(4), 631–648, DOI: **10.1080/08843759408916198**.

36 J. I. Mujika, J. Uranga and J. M. Matxain, Computational Study on the Attack of OH Radicals on Aromatic Amino Acids, *Chem. – A Eur. J.*, 2013, **19**(21), 6862–6873, DOI: **10.1002/chem.201203862**.

37 D. Petrov, D. Tunega, M. H. Gerzabek and C. Oostenbrink, Molecular Dynamics Simulations of the Standard Leonardite Humic Acid: Microscopic Analysis of the Structure and Dynamics, *Environ. Sci. Technol.*, 2017, **51**(10), 5414–5424, DOI: **10.1021/acs.est.7b00266**.

38 F. Yang and M. Antonietti, *The Sleeping Giant: A Polymer View on Humic Matter in Synthesis and Applications. Progress in Polymer Science*, Elsevier Ltd, 2020, p. 101182, DOI: **10.1016/j.progpolymsci.2019.101182**.

39 S. V. Sancheti and P. R. Gogate, A Review of Engineering Aspects of Intensification of Chemical Synthesis Using Ultrasound, *Ultrason. Sonochem.*, 2017, **36**, 527–543, DOI: 10.1016/J.ULTSONCH.2016.08.009.

40 M. A. Sabar, M. I. Ali, N. Fatima, A. Y. Malik, A. Jamal, R. Liaquat, H. He, F.-J. Liu, H. Guo, M. Urynowicz and Z. Huang, Evaluation of Humic Acids Produced from Pakistani Subbituminous Coal by Chemical and Fungal Treatments, *Fuel*, 2020, **278**, 118301, DOI: 10.1016/j.fuel.2020.118301.

41 P. Zhu, Z. Wang, C. Pan, Z. K. Li, W. Zhang, J. Yan, S. Kang, S. Ren, Z. Lei, J. Zhao and H. Shui, Investigation of Hydrothermal Depolymerization of Lignite under Different Conditions by 13C NMR Spectroscopy, *J. Anal. Appl. Pyrolysis*, 2024, **180**, 106562, DOI: 10.1016/J.JAAP.2024.106562.

42 E. V. Rokhina, P. Lens and J. Virkutyte, Low-Frequency Ultrasound in Biotechnology: State of the Art, *Trends Biotechnol.*, 2009, **27**(5), 298–306, DOI: 10.1016/J.TIBTECH.2009.02.001.

43 A. A. Pájaro-Payares, E. A. Espinosa-Fuentes, F. Colpas-Castillo, J. Rodríguez-Ruiz, R. Fernández-Maestre and E. Meza-Fuentes, Effect of Particle Size and Oxidant Concentration in the Yield of Humic Acids from Mineral Coal Using Response Surface Methodology, *Rev. la Acad. Colomb. Ciencias Exactas, Fis. y Nat.*, 2017, **41**(160), 306–313, DOI: 10.18257/raccefyn.477.

44 G. Mesri, M. Asce, M. Ajlouni and A. M. Asce, Engineering Properties of Fibrous Peats, *J. Geotech. Geoenvironmental Eng.*, 2007, **133**(7), 850–866, DOI: 10.1061/(ASCE)1090-0241(2007)133:7(850).

45 D. Garcia, J. Cegarra, M. Abad and F. Fornes, Effects of the Extractants on the Characteristics of a Humic Fertilizer Obtained from Lignite, *Bioresour. Technol.*, 1993, **43**(3), 221–225, DOI: 10.1016/0960-8524(93)90034-9.

46 T. Jaing, G. Han, Y. Zhang, Y. Huang, G. Li, Y. Guo and Y. Yang, Improving Extraction Yield of Humic Substances from Lignite with Anthraquinone in Alkaline Solution, *J. Cent. South Univ. Technol.*, 2011, **18**(1), 68–72, DOI: 10.1007/s11771-011-0660-3.

47 M. Tatzber, M. Stemmer, H. Spiegel, C. Katzlberger, G. Haberhauer, A. Mentler and M. H. Gerzabek, FTIR-Spectroscopic Characterization of Humic Acids and Humin Fractions Obtained by Advanced NaOH, Na4P2O7, and Na2CO3 Extraction Procedures, *J. Plant Nutr. Soil Sci.*, 2007, **170**(4), 522–529, DOI: 10.1002/JPLN.200622082.

48 L. J. Huey, Effects of Extractants on the Yields and Selected Chemical Characteristics of Humic Acids Isolated from Tropical Saprists Peat, *Am. J. Appl. Sci.*, 2010, **7**(7), 933–936, DOI: 10.3844/ajassp.2010.933.936.

49 Y. Li and S. Yuan, Influence of Addition of KOH on the Yield and Characteristics of Humic Acids Extracted from Lignite Using NaOH, *SN Appl. Sci.*, 2021, **3**(1), 47, DOI: 10.1007/s42452-020-04087-x.

50 J. Du, N. Sato and O. Tochiyama, Potentiometric Study on the Proton Binding of Humic Substances, *J. Nucl. Radiochem. Sci.*, 2005, **6**(1), 25–29, DOI: 10.14494/JNRS2000.6.25.

51 A. Eladeb, A. Aydi and I. Alenezi, Ethanolysis of Waste Cooking Oils Using KOH Catalyst, *Orient. J. Chem.*, 2021, **37**(6), 1344–1349, DOI: 10.13005/OJC/370611.

52 S. H. Hegdahl, C. Løhre and T. Barth, Hydrothermal Liquefaction of Sewage Sludge Anaerobic Digestate for Bio-Oil Production: Screening the Effects of Temperature, Residence Time and KOH Catalyst, *Waste Manag. Res. J. a Sustain. Circ. Econ.*, 2023, **41**(5), 977–986, DOI: 10.1177/0734242X221138497.

53 J. Salimon, B. M. Abdullah and N. Salih, Hydrolysis Optimization and Characterization Study of Preparing Fatty Acids from Jatropha Curcas Seed Oil, *Chem. Cent. J.*, 2011, **5**(1), 67, DOI: 10.1186/1752-153X-5-67.

54 F. Boylu, H. Dinçer and G. Ateşok, Effect of Coal Particle Size Distribution, Volume Fraction and Rank on the Rheology of Coal-Water Slurries, *Fuel Process. Technol.*, 2004, **85**(4), 241–250, DOI: 10.1016/S0378-3820(03)00198-X.

55 M. Klučáková, Mean Activity Coefficients of Humic Acids as Physicochemical Characteristics of Their Behavior in Water Environment, *ACS Omega*, 2020, **5**(49), 31518–31524, DOI: 10.1021/ACSOMEGA.0C03311/ASSET/IMAGES/LARGE/AO0C03311_0008.JPEG.

56 T. Rashid, F. Sher, M. Jusoh, T. A. Joya, S. Zhang, T. Rasheed and E. C. Lima, Parametric Optimization and Structural Feature Analysis of Humic Acid Extraction from Lignite, *Environ. Res.*, 2023, **220**, 115160, DOI: 10.1016/J.ENVRES.2022.115160.

57 Y. Xu and S. Pan, Effects of various factors of ultrasonic treatment on the extraction yield of all-trans-lycopene from red grapefruit (Citrus paradisi Macf.), *Ultrason. Sonochem.*, 2013, **20**, 1026–1032, DOI: 10.1016/j.ultsonch.2013.01.006.

58 Z. Kobus, Dry Matter Extraction from Valerian Roots (Valeriana Officinalis L.) with the Help of Pulsed Acoustic Field, *Int. Agrophysics*, 2008, **22**(2), 133–137.

59 R. Kadkhodaee and A. Hemmati-Kakhki, Ultrasonic Extraction of Active Compounds from Saffron, *Acta Hortic*, 2007, **739**, 417–425, DOI: 10.17660/ACTAHORTIC.2007.739.55.

60 T. Tuziuti, K. Yasui, J. Lee, T. Kozuka, A. Towata and Y. Iida, Mechanism of Enhancement of Sonochemical-Reaction Efficiency by Pulsed Ultrasound, *J. Phys. Chem. A*, 2008, **112**(22), 4869–4874, DOI: 10.1021/jp802640x.

61 H. Mitome and S. I. Hatanaka, Optimization of a Sonochemical Reactor Using a Pulsing Operation, in *Ultrasonics*, 2002, Vol. 40, DOI: 10.1016/S0041-624X(02)00258-5.

62 E. J. Hart and A. Henglein, Free Radical and Free Atom Reactions in the Sonolysis of Aqueous Iodide and Formate Solutions, *J. Phys. Chem.*, 1985, **89**(20), 4342–4347, DOI: 10.1021/j100266a038.

63 J. Liu, F. Yang, J. Xia, F. Wu and C. Pu, Mechanism of ultrasonic physical-chemical viscosity reduction for different heavy oils, *ACS Omega*, 2021, **6**, 3933–3941, DOI: 10.1021/acsomega.0c05585.

64 M. Stefanescu, G. Nechifor, C. Bumbac, I. Ionescu and O. Tiron, Improvement of Active Biological Sludge Quality for Anaerobic Digestion Phase in the Wastewater Treatment Plant by Ultrasonic Pretreatment, *Rev. Chim.*, 2018, **69**(1), 31–33, DOI: 10.37358/RC.18.1.6039.

65 A. Jatnika Effendi and M. Wulandari The Impact of Ultrasonic Power and Time for the Removal of Total Petroleum Hydrocarbon from Low Permeability Contaminated Soils, in *IOP Conference Series: Earth and Environmental Science*, 2019; Vol. 314, DOI: 10.1088/1755-1315/314/1/012005.

66 J. Liao, N. Zheng and B. Qu, An Improved Ultrasonic-Assisted Extraction Method by Optimizing the Ultrasonic Frequency for Enhancing the Extraction Efficiency of Lycopene from Tomatoes, *Food Anal. Methods*, 2016, **9**(8), 2288–2298, DOI: 10.1007/S12161-016-0419-4/TABLES/2.

67 Y. Asakura, S. Fukutomi, K. Yasuda and S. Koda, Optimization of Sonochemical Reactors by Measuring Impedance of Transducer and Sound Pressure in Solution, *Chem. Eng. Japan*, 2010, **43**(12), 293–297, DOI: 10.1252/jcej.10we158.

68 I. Nishida, Precipitation of Calcium Carbonate by Ultrasonic Irradiation, *Ultrason. Sonochem.*, 2004, **11**(6), 423–428, DOI: 10.1016/j.ultsonch.2003.09.003.

69 A. V. Mohod and P. R. Gogate, Ultrasonic Degradation of Polymers: Effect of Operating Parameters and Intensification Using Additives for Carboxymethyl Cellulose (CMC) and Polyvinyl Alcohol (PVA), *Ultrason. Sonochem.*, 2011, **18**(3), 727–734, DOI: 10.1016/j.ultsonch.2010.11.002.

70 J. Klíma, A. Frias-Ferrer, J. González-García, J. Ludvík, V. Sáez, J. Iniesta and J. Heyrovský, Optimisation of 20 kHz sonoreactor geometry on the basis of numerical simulation of local ultrasonic intensity and qualitative comparison with experimental results, *Ultrason. Sonochem.*, 2006, **13**(1), 42–49, DOI: 10.1016/j.ultsonch.2006.01.001.

71 Y. Sun, D. Liu, J. Chen, X. Ye and D. Yu, Effects of Different Factors of Ultrasound Treatment on the Extraction Yield of the All-Trans-β-Carotene from Citrus Peels, *Ultrason. Sonochem.*, 2011, **18**, 243–249, DOI: 10.1016/j.ultsonch.2010.05.014.

72 Y. Kojima, H. Imazu and K. Nishida, Physical and Chemical Characteristics of Ultrasonically-Prepared Water-in-Diesel Fuel: Effects of Ultrasonic Horn Position and Water Content, *Ultrason. Sonochem.*, 2014, **21**(2), 722–726, DOI: 10.1016/j.ultsonch.2013.09.019.

73 A. D. Manasrah, G. Vitale and N. N. Nassar, Catalytic Oxy-Cracking of Petroleum Coke on Copper Silicate for Production of Humic Acids, *Appl. Catal. B Environ.*, 2020, **264**, 118472, DOI: 10.1016/j.apcatb.2019.118472.

74 S. Zhang, L. Yuan, W. Li, Z. Lin, Y. Li, S. Hu and B. Zhao, Characterization of PH-Fractionated Humic Acids Derived from Chinese Weathered Coal, *Chemosphere*, 2017, **166**, 334–342, DOI: 10.1016/J.CHEMOSPHERE.2016.09.095.

75 M. Huculak-Mączka, J. Hoffmann and K. Hoffmann, Evaluation of the Possibilities of Using Humic Acids Obtained from Lignite in the Production of Commercial Fertilizers, *J. Soils Sediments*, 2018, **18**(8), 2868–2880, DOI: 10.1007/s11368-017-1907-x.

76 D. S. Volkov, O. B. Rogova and M. A. Proskurnin, Temperature Dependences of IR Spectra of Humic Substances of Brown Coal, *Agron*, 2021, **11**(9), 1822, DOI: 10.3390/AGRONOMY11091822.

77 R. Al-Akbari, M. Razi, I. Badran and N. N. Nassar, Thermo-Oxidative Conversion of PDC as a Molecular Model of Residual Feedstocks to Oxygen-Rich Chemicals, *React. Chem. Eng.*, 2023, **8**(5), 1083–1096, DOI: 10.1039/D3RE00036B.

78 F. Stevenson, *Humus Chemistry: Genesis, Composition, Reactions*, Wiley, 1994.

79 K. H. Tan, *Humic Matter in Soil and the Environment: Principles and Controversies*, CRC Press, 2003, DOI: 10.1201/9780203912546.

80 J. D. Ritchie and E. M. Perdue, Analytical Constraints on Acidic Functional Groups in Humic Substances, *Org. Geochem.*, 2008, **39**(6), 783–799, DOI: 10.1016/j.orggeochem.2008.03.003.

81 J. D. Ritchie and E. Michael Perdue, Proton-Binding Study of Standard and Reference Fulvic Acids, Humic Acids, and Natural Organic Matter, *Geochim. Cosmochim. Acta*, 2003, **67**(1), 85–96, DOI: 10.1016/S0016-7037(02)01044-X.

82 H. Li, S. Liang, Y. Hou, Y. Wang, S. Ren and W. Wu, A Study on the Structure of Naomaohu Coal and Its Suitability for Direct Coal Liquefaction, *Fuel Process. Technol.*, 2022, **227**, 107298, DOI: 10.1016/j.fuproc.2021.107135.

83 Y. Xu, Q. Fu, Y. Hong, Y. Zhang, L. Wang, K. Bei, I. M. Chou, H. Hu and Z. Pan, Effects of Vitrinite in Low-Rank Coal on the Structure and Combustion Reactivity of Pyrolysis Chars, *ACS Omega*, 2020, **5**(28), 17314–17323, DOI: 10.1021/acsomega.0c01542.

84 X. Qin, T. Yang, Z. Liu and Q. Liu, Molecular Structure, Bond Cleavage and Their Relation of Four Low Rank Coals, *Fuel Process. Technol.*, 2022, **236**, DOI: 10.1016/j.fuproc.2022.107391.

85 K. Qin and D. I. Leskovar, Assessments of Humic Substances Application and Deficit Irrigation in Triploid Watermelon, *HortScience*, 2020, **55**(5), 677–683, DOI: 10.21273/HORTSCI14872-20.

86 T. B. Edil and A. Dhowian, At-Rest Lateral Pressure of Peat Soils, *Journal of the Geotechnical Engineering Division*, 1981, **107**, 201–218, DOI: 10.1061/ajgeb6.0001097.

87 M. Xuehui and H. Jinming, in *Coal, Oil Shale, Natural Bitumen, Heavy Oil and Peat*; 2009; Vol. 2.

88 W. K. Davis and V. K. Diessel, Graphical-Statistical Method for the Study of Structure and Reaction Processes of Coal, *Fuel*, 1950, **29**, 269–284, DOI: 10.20710/DOJO.81.2_162.

89 A. D. Manasrah, A. El-Qanni, I. Badran, L. Carbognani Ortega, M. J. Perez-Zurita and N. N. Nassar, Experimental and Theoretical Studies on Oxy-Cracking of Quinolin-65 as a Model Molecule for Residual Feedstocks, *React. Chem. Eng.*, 2017, **2**(5), 709–719, DOI: 10.1039/c7re00048k.

90 N. A. Khan, N. Fujitake, Y. Noda, T. Suzuki and H. Otsuka, Comparison of Humic Acid Fractions Derived from

Thermally Created Plant Residues and Natural Soils: Spectroscopic and Elemental Analyses, *Soil Sci. Plant Nutr.*, 2006, **52**(3), 279–287, DOI: **10.1111/j.1747-0765.2006.00044.x**.

91 S. L. Maunu, NMR Studies of Wood and Wood Products, *Prog. Nucl. Magn. Reson. Spectrosc.*, 2002, **40**(2), 151–174, DOI: **10.1016/S0079-6565(01)00041-3**.

92 E. Abakumov, E. Lodygin and V. Tomashunas, 13C NMR and ESR Characterization of Humic Substances Isolated from Soils of Two Siberian Arctic Islands, *Int. J. Ecol.*, 2015, **2015**, 1–7, DOI: **10.1155/2015/390591**.

93 K. A. Thorn, D. W. Folan and P. MacCarthy, *U.S. Geological Survey Water-Resources Investigations Report*, 1989, DOI: **10.3133/WRI894196**.

94 A. D. Manasrah, A. Hassan and N. N. Nassar, Enhancement of Petroleum Coke Thermal Reactivity Using Oxy-Cracking Technique, *Can. J. Chem. Eng.*, 2019, **97**(11), 2794–2803, DOI: **10.1002/cjce.23574**.

95 H. Kühl, M. M. Kashani-Motlagh, H. J. Mühlen and K. H. van Heek, Controlled Gasification of Different Carbon Materials and Development of Pore Structure, *Fuel*, 1992, **71**(8), 987–992, DOI: **10.1016/0016-2361(92)90236-H**.

96 T. W. Kwon, S. D. Kim and D. P. C. Fung, Reaction Kinetics of Char-CO2 Gasification, *Fuel*, 1988, **67**(4), 546–550, DOI: **10.1016/0016-2361(88)90350-X**.

97 E. B. Flint and K. S. Suslick, The Temperature of Cavitation, *Science*, 1991, **253**(5026), 1397–1399, DOI: **10.1126/science.253.5026.1397**.

98 K. S. Suslick Sonochemistry, in *Comprehensive Coordination Chemistry II*, 2004, Vol. 1, DOI: **10.1016/B0-08-043748-6/01046-X**.

99 J. P. Lorimer and T. J. Mason, Sonochemistry. Part 1 - The Physical Aspects, *Chemical Society Reviews*, 1987, **16**, 239–274, DOI: **10.1039/CS9871600239**.

100 J. G. Lin, C. N. Chang, J. R. Wu and Y. S. Ma, Enhancement of Decomposition of 2-Chlorophenol with Ultrasound/H2O2 Process, *Water Science and Technology*, 1996, **34**(9), 291–298, DOI: **10.1016/S0273-1223(96)00785-8**.

101 M. R. Hoffmann, I. Hua and R. Höchemer, Application of Ultrasonic Irradiation for the Degradation of Chemical Contaminants in Water, *Ultrason. Sonochem.*, 1996, **3**(3), S163–S172, DOI: **10.1016/S1350-4177(96)00022-3**.

102 I. Hua, R. H. Hoechemer and M. R. Hoffmann, Sonolytic Hydrolysis of P-Nitrophenyl Acetate. The Role of Supercritical Water, *J. Phys. Chem.*, 1995, **99**(8), 2335–2342, DOI: **10.1021/j100008a015**.

103 A. Tauber, H. P. Schuchmann and C. Von Sonntag, Sonolysis of Aqueous 4-Nitrophenol at Low and High PH, *Ultrason. Sonochem.*, 2000, **7**, 45–52, DOI: **10.1016/S1350-4177(99)00018-8**.

104 A. G. Hardie, Pathways of Abiotic Humification as Catalyzed by Mineral Colloids, PhD thesis, University of Saskatchewan, 2008.